Inorganic Chemistry

pubs.acs.org/IC Article

Probing Magnetic Anisotropy in $(NBu^n_4)_2[ReX_6]$ (X = Cl, Br, I): Ligand Field of the Re^{IV}-Halide Bonds in Distorted Octahedral Complexes

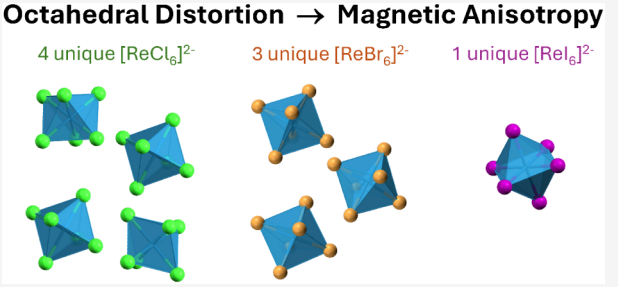
Published as part of Inorganic Chemistry special issue "Pushing the Limits of Molecular Magnetism".

Adam T. Hand, Alexandria N. Bone, Shashank V. Rao, Brandon D. Watson-Sanders, Adiat A. Fakolujo, Yongqiang Cheng, Mykhaylo Ozerov, J. Krzystek, Zheng Gai, Wei Lv, Xue-Tai Chen, You Song, Luke L. Daemen, Xiaoping Wang, Mihail Atanasov,* Frank Neese, and Zi-Ling Xue*

Cite This: *Inorg. Chem.* 2026, 65, 24492−24504 Read Online

ACCESS | Metrics & More | Article Recommendations | Supporting Information

ABSTRACT: In six-coordinate complexes with $S \geq 1$, deviations from perfect O_h geometry lead to magnetic anisotropy. We have studied $(NBu^n_4)_2[Re^{IV}X_6]$ (**Re−X**; X = Cl, Br, I; $S = 3/2$), including zero-field splitting (ZFS) in **Re−I**, by advanced spectroscopies [far-IR magneto-spectroscopy (FIRMS), high-frequency and -field EPR (HFEPR), and inelastic neutron scattering (INS)]. AC susceptibility of **Re−I** shows field-induced SMM (single-molecule magnet) properties. Unlike **Re−I** with one unique $[ReI_6]^{2-}$ center, there are four and three different $[ReX_6]^{2-}$ centers in the crystallographic unit cells of **Re−Cl** and **Re−Br**, respectively. *Ab initio* calculations determine ZFS parameters and show that magnetic anisotropies are influenced by deviations from the O_h geometry and by increased covalency from **Re−Cl** to **Re−Br** to **Re−I**. Although Re−X bond lengths increase from **Re−Cl** to **Re−Br** to **Re−I**, the calculations reveal that the longer Re−I bonds are compensated by the diffuse, better-overlapping orbitals of I^- ligands. The diffuseness in ligand orbitals likely contributes to the SMM performance of **Re−I**. The calculations also indicate that deviations from the O_h geometry in $[ReX_6]^{2-}$ ions are the sole source of magnetic anisotropy and that there is no heavy-atom effect from the halide ligands. Spin-phonon couplings in **Re−I** have been probed by FIRMS using results from DFT phonon calculations.



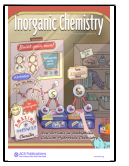
INTRODUCTION

Hexahalorhenates $[ReX_6]^{2-}$ (X = F, Cl, Br, I) have been studied since the 1960s,[1−13] including their *d-d* absorption and charge-transfer spectra as indirect sources of information about the Re−X bond, based on ligand-field parameters derived from the spectra.[1,2] These Re^{IV} complexes with three unpaired electrons ($S = 3/2$) have been of recent interest as single-molecule magnets (SMMs),[14−25] exhibiting an energy barrier to the relaxation of magnetization (U_{eff}) with applications in high-density storage devices and qubits in spintronics.[26−46] One strategy for designing SMMs involves the use of heavy transition-metal ions.[14,15,41,47−56] Complexes of heavier 4*d*/5*d* metal ions exhibit strong spin-orbit coupling (SOC)[57] and extended valence orbitals, making them promising SMMs.[41]

Among 5*d* transition metals, Re^{IV}-based complexes, such as clusters and single-chain magnets, are leading candidates for SMMs.[41,51,58−60] However, the number of reported Re^{IV}-based *mononuclear* SMMs (also known as single-ion magnets, SIMs) is limited. The highly anisotropic $(NBu^n_4)_2[ReX_4(ox)]$ (ox = oxalate; X = Cl or Br)[49] complexes are prime examples of Re^{IV} SMMs.[23,50] The magnetic properties of mononuclear transition-metal complexes result from structural deviations from a perfect O_h or T_d ligand field and are influenced by the SOC of the unpaired electrons in the complexes.[61]

Octahedral $[ReX_6]^{2-}$ complexes are ideal for probing how structural deviations and the heavy metal atom affect their magnetic properties. The deviations remove the *d*-orbital degeneracies, leading to zero-field splitting (ZFS) of the quartet spin state ($2S + 1 = 4$) into two Kramers doublets, $M_S = \pm 1/2$ and $M_S = \pm 3/2$,[31,61] due to second-order SOC.[61−63] In $[ReX_6]^{2-}$, ZFS leads to the splitting of the $^4A_{2g}$ ground state (Figure 1). SOC is stronger for heavy atoms.[64,65] Sarkar, Rajaraman, and coworkers have used *ab initio* ligand-field analyses to study magnetic anisotropy in tetrahedral $Co^{II}X_4$ complexes (X = O, S, Se, with the chalcogen atoms bonded to the Co^{II} ion),[66] showing that structural factors are more important than the presence of heavy atoms.

Received: August 6, 2026
Revised: September 3, 2026
Accepted: September 9, 2026
Published: October 2, 2026



ACS Publications

© 2026 The Authors. Published by American Chemical Society

Downloaded from pubs.acs.org/inoaj/article-pdf/65/41/24492/6873108/acs.inorgchem.6c04158.pdf by FLORIDA STATE UNIV user on 02 November 2026

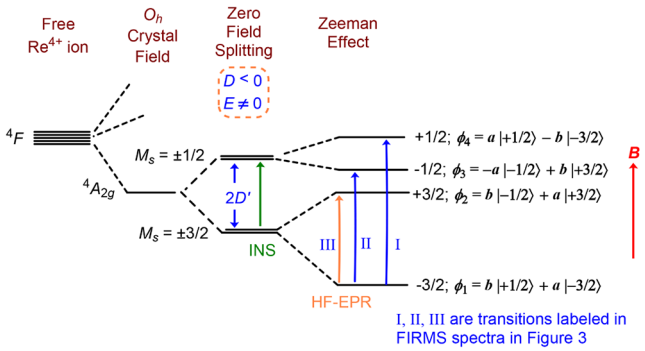


Figure 1. Splitting in **Re−Cl** and **Re−I** with easy-axis ($D < 0$) anisotropy and $E \neq 0$. For **Re−Br** with easy-plane ($D > 0$) anisotropy and $E \neq 0$, the energy of the $M_S = \pm 1/2$ level is lower than that of $M_S = \pm 3/2$. D and E are axial and rhombic ZFS parameters, respectively. $2D' = 2(D^2 + 3E^2)^{1/2}$.[15,50,51,67] The spectroscopies in the current work are marked. When $E \neq 0$, mixing of the $M_S = \pm 1/2$ and $M_S = \pm 3/2$ states occurs with $\tan(2\beta) = \sqrt{3}(E/D)$.[68,69] As a result, the $M_S = \pm 1/2$ character in the $M_S = \mp 3/2$ states makes the $\phi_1 \rightarrow \phi_2$ transition spin-allowed.

The spin Hamiltonian for an $S = 3/2$ complex[61] is given in eq 1:

$$\hat{H}_S = D\left(\hat{S}_z^2 - \frac{5}{4}\right) + E(\hat{S}_x^2 - \hat{S}_y^2) + \mu_B g_x B_x \hat{S}_x + \mu_B g_y B_y \hat{S}_y + \mu_B g_z B_z \hat{S}_z \quad (1)$$

where $\hat{S}$ = spin operator; μ_B = Bohr magneton; g_x, g_y, g_z (also written as g_{xx}, g_{yy}, g_{zz}; $g = [g_x, g_y, g_z]$) = g-factor components; (B_x, B_y, B_z) = components of the magnetic induction vector $\boldsymbol{B}$.

Rojas−Dotti, Martinez-Lillo, and coworkers have shown slow magnetic relaxation in $(PPh_4)_2[ReX_6]$ (X = Br and I) and studied their ZFS by magnetometry.[15] Re-based SMMs with *multicenter* heterometallic structures, containing both Re^{II} and Re^{IV} complexes and other paramagnetic ions such as Mn^{II}, Co^{II}, Ni^{II}, and Cu^{II}, have also been studied.[58−60] Their magnetic properties must be attributed to the large SOC of Re ions and low symmetry, leading to larger ground-state spins.

We have focused on the simpler $[ReX_6]^{2-}$ complexes to clearly understand the connections between electronic and geometric structures and their magnetic and spectroscopic properties, both experimentally and theoretically. The complexes have been studied with the following interests: (1) How is the deviation from the perfect O_h ligand field reflected in magnetic anisotropy (i.e., ZFS) in the complexes? (2) What are the natures of the Re−X bonds from the perspective of ligand field theory? (3) Is there a heavy-atom effect on ZFS for the complexes containing six heavy halide ligands, or are the deviations from the perfect O_h ligand field the only source of ZFS in the complexes? (4) Could the degree of ZFS, i.e., $2D'$ and spin-Hamiltonian (SH) parameters, be determined by a combined use of advanced spectroscopies, including far-IR magneto-spectroscopy (FIRMS), high-frequency and -field EPR (HFEPR), and inelastic neutron scattering (INS)? (5) Could magnetic relaxation in the complexes be probed through studies of spin-phonon coupling in FIRMS and AC (alternating-current) magnetic susceptibility? Herein we report comprehensive studies of $(NBu^n_4)_2[ReX_6]$ [X = Cl (**Re−Cl**), Br (**Re−Br**), I (**Re−I**)] to provide answers to these questions.[20,44,45,67,70−81] DC (direct-current) susceptibilities of the complexes have also been studied. **Re−I** demonstrates SMM behavior, and its phonon properties (i.e., energies, symmetries, and movies) have been obtained through DFT (density functional theory) calculations using the Vienna Ab initio Simulation Package (VASP).

RESULTS AND DISCUSSION

Single-Crystal Structures and SHAPE Analyses

Single-crystal structures of **Re−Cl**, **Re−Br**, and **Re−I** at 100 K from X-ray diffraction have been obtained. Selected bond lengths and angles are given in Table 1, while the complete list of crystallographic data and structure refinement parameters is given in Table S1. **Re−Cl** crystallizes in the triclinic $P\bar{1}$ (No. 2) space group (CCDC deposition no. 2348938). Each crystallographic unit cell contains eight **Re−Cl** molecules, four of which are unique. Re−Cl bond lengths vary by 0.04 Å, and *cis* Cl−Re−Cl angles by 2.7°. **Re−Br** crystallizes in the monoclinic C_2/c (No. 15) space group (CCDC deposition No.: 2348939). Each crystallographic unit cell contains 16 **Re−Br** molecules, three of which are unique. Re−Br bond lengths vary by 0.07 Å, and *cis* Br−Re−Br angles by 7.8°. Similar crystal structures of Ir^{IV} (100 K)[82] and Pt^{IV} (150 K)[83] analogs of **Re−Br** have been reported. **Re−I** crystallizes in the monoclinic $P2_1/n$ (No. 14) space group (CCDC deposition No.: 2348940). Each crystallographic unit cell contains four equivalent (*i.e.*, one unique) **Re−I** molecules. The structure of the $[ReI_6]^{2-}$ anion is shown in Figure 2. Re−I bond lengths vary by 0.05 Å, and *cis* I−Re−I angles by 2.5°. Re−X bond distances increase in the order of Cl < Br < I, reflecting the

Table 1. Selected Bond Lengths and Angles

	Re−Cl	Re−Br	Re−I
Re−X length	2.3367(9)−2.3778(6)	2.4728(17)−2.5315(9)	2.7060(3)−2.7562(3)
cis X−Re−X angle (°)	88.53(3)−91.19(2)	86.1(2)−93.9(2)	88.832(9)−91.322(9)
trans X−Re−X angle (°)	177.83(3)−179.80(3)	172.2(5)−180.0	178.259(8)−179.836(8)
Shortest Re···Re distance (Å)	9.5231(9)	9.7387(0)	9.7896(5)

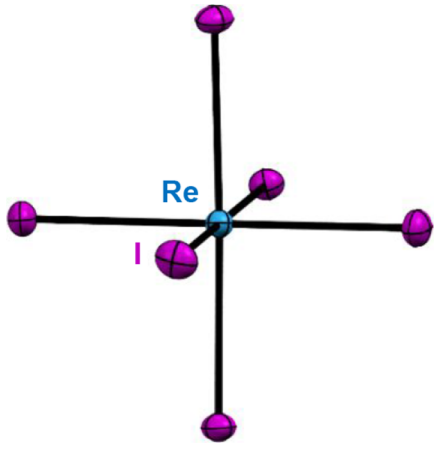


Figure 2. Crystal structure of the $[ReI_6]^{2-}$ anion in **Re−I**. Thermal ellipsoids are depicted at the 50% probability level. Representative crystal structures of the $[ReCl_6]^{2-}$ and $[ReBr_6]^{2-}$ anions in **Re−Cl** and **Re−Br** are given in Figure S2.

Downloaded from pubs.acs.org/inoaaj/article-pdf/65/41/24492/6737108/acs.inorgchem.6c04158.pdf by FLORIDA STATE UNIV user on 02 November 2026

https://doi.org/10.1021/acs.inorgchem.6c04158
Inorg. Chem. 2026, 65, 24492−24504

Table 2. Summary of Spin-Hamiltonian (SH) Parameters for Re−Cl, Re−Br, and Re−I from CASSCF/NEVPT2 Calculations and Spectroscopies for Re−I

Complex	Method[a]	g	D (cm^{-1})	$\lvert E\rvert$ (cm^{-1})	$\lvert E/D\rvert$	$2D'$ (cm^{-1})
Re−I	Spectroscopies	[1.9, 1.9, 1.8]	−13.1[b]	3.02[b]	0.23	28.3(5)
	Calculations	[1.8, 1.8, 1.8]	5.39	1.20	0.22	11.6
Re−Br	Calculations					
	Re(1)	[1.8, 1.8, 1.8]	1.11	0.06	0.05	2.23
	Re(8)	[1.8, 1.8, 1.8]	7.65	1.90	0.24	17.19
	Re(15)	[1.8, 1.8, 1.8]	6.81	1.14	0.17	14.18
Re−Cl	Calculations					
	Re(2)	[1.8, 1.8, 1.8]	−4.21	−0.50	0.12	8.60
	Re(61)	[1.8, 1.8, 1.8]	−8.67	−2.05	0.24	18.74
	Re(121)	[1.8, 1.8, 1.8]	7.90	2.31	0.29	17.72
	Re(234)	[1.8, 1.8, 1.8]	5.15	1.35	0.26	11.31

[a]The spectroscopic data for $[ReI_6]^{2-}$ (**Re−I**) refer to the parameters determined from HFEPR, FIRMS, and INS. Calculations refer to computed parameters derived from CASSCF/NEVPT2, giving values for each magnetically inequivalent Re^{IV} center in the unit cell. [b]For the spectroscopic methods, D and E values are determined through the E/D ratio from HFEPR and $2D'$ from FIRMS and INS. The sign of D is based on the HFEPR results. $2D'$ values from FIRMS and INS were found to be identical.

increase in ionic radii from Cl to I. The structural data are similar to the $(PPh_4)_2[ReX_6]$ (X = Br, I) analogs reported by Rojas−Dotti, Martinez-Lillo, and coworkers.[15]

Structures of the complexes deviate from the perfect O_h symmetry in part because of the $NBu^n{}_4^+$ cations, giving rise to ZFS. Deviations of $[ReX_6]^{2-}$ anions in **Re−Cl**, **Re−Br**, and **Re−I** by *SHAPE* are given in Table S4.[84] **Re−Br** shows the largest average distortion from O_h, followed by **Re−I**, with **Re−Cl** as the least distorted. This feature is probably associated with the σ-bonding energy in **Re−Br**, as discussed below, where the decrease in bond energy allows for greater distortion. Minimal-distortion interconversion pathways between O_h and several other geometries (e.g., trigonal prism)[85,86] have also been analyzed by *SHAPE*.[84] Such a pathway is the interconversion route between two ideal geometries with minimal distortion.[84,85] The assignment of an ideal polyhedron to an observed structure is typically challenging. Thus, the analysis of the pathways by *SHAPE* offers a useful description of the observed structure, giving the percentage of distortion/conversion, known as the generalized interconversion coordinate, from O_h to other possible shapes of six-coordinate complexes.[86] The results, including Figure S16, are given in the Supporting Information (SI). For **Re−Cl**, distortions of its four unique Re^{IV} sites from O_h range from 0.9% to 2.8%, which are slightly smaller than 2.1−3.1% observed for the single Re^{IV} site in **Re−I**. The three unique sites in **Re−Br** show 3.1%−8.0% distortions.

The *SHAPE* analysis gives deviations of Re−X bond lengths from the average, as well as of *cis* (α') and *trans* (β') angles from 90° and 180°, respectively, yielding more detailed information about the distortion from the ideal O_h symmetry (Table S4). The data suggest that distortions along the *cis* (α') and *trans* (β') angles dominate the lowering of the O_h symmetry, with values of $\delta\alpha'$ and $\delta\beta'$ decreasing from **Re−Br** to **Re−Cl** and then **Re−I**. There is no systematic correlation with respect to variations in the sign and magnitude of D. We thus decided to compute the SH parameters using CASSCF/NEVPT2 and **Re−X** geometries from X-ray data. These are included in Table 2, in comparison with the experimental values . For **Re−I** with a unique $[ReI_6]^{2-}$ unit, D turns out to be positive in the calculations, implying easy-plane anisotropy superimposed by a sizable rhombic E/D ratio (0.22). Positive but widely varying values of calculated D for the three different Re(1), Re(8), and Re(15) sites in **Re−Br** (1.11, 7.65, and 6.81 cm^{-1}, respectively) result in sizable and variable rhombic E/D ratios among the different sites. For the four different Re sites of **Re−Cl**, varying signs of D are computed [−4.21, −8.67, 7.90, and 5.15 cm^{-1} for Re(2), Re(61), Re(121), and Re(234), respectively], with large rhombic E/D ratios, which are close to the limiting value of E/D = 1/3 for the Re(121) site (0.29). Results of the calculations indicate that all three complexes deviate significantly from the limit of a D_{4h} axial geometry, which is important for the magnetic properties. We have also analyzed whether there is a correlation between the distortions along different minimal-distortion interconversion pathways in **Re−Cl**, **Re−Br**, or **Re−I** and their ZFS values. The analysis is given in the SI (Figure S16 and Table S5).

FIRMS, HFEPR, and INS

The magnetic transitions between the M_S = ±3/2 and M_S = ±1/2 levels, shown in Figure 1, have been probed using powder samples by FIRMS and HFEPR (two advanced spectroscopies at the National High Magnetic Field Laboratory (NHMFL)) and by INS on VISION (Vibrational Spectrometer) at Oak Ridge National Laboratory (ORNL).[87] The spectroscopic studies of **Re−I** have also yielded its SH parameters (D, E, and g). The transitions between the M_S levels are magnetic dipole-allowed.[88,89] The use of FIRMS, HFEPR, and INS to study magnetic anisotropy has been recently reviewed.[79,87,90]

In FIRMS, the energy range of 12−720 cm^{-1} is probed at 0−17 T. Magnetic transitions in Figure 1 shift in energy with changes in the field due to the Zeeman effect, while phonons do not. Thus, FIRMS helps identify magnetic transitions, yielding $2D' = 2(D^2 + 3E^2)^{1/2}$ values from the spectra. Using powder samples in the current work made the experiments relatively easier to conduct than using single crystal samples. However, obtaining additional information such as the E/D ratio or g values requires the use of other techniques such as HFEPR.[87] Here, phonons refer to both external (intermolecular) and internal (intramolecular) vibrations.[91−93] Internal and external modes often couple as they originate from the same governing equations.[92,93] Thus, we do not distinguish between external and internal modes in the current work and refer to all vibrations as phonons.

https://doi.org/10.1021/acs.inorgchem.6c04158
Inorg. Chem. 2026, 65, 24492−24504

Downloaded from pubs.acs.org/inoaaj/article-pdf/65/41/24492/6873108/acs.inorgchem.6c04158.pdf by FLORIDA STATE UNIV user on 02 November 2026

In HFEPR, the energy of the transition is fixed (e.g., at a frequency of 68 GHz, corresponding to 2.3 cm^{-1}), and the magnetic field is swept from 0 to 14.5 T to observe the transition from the M_S = −3/2 state to the M_S = +3/2 state (within the M_S = ±3/2 doublet). Using the 2D' value from FIRMS (and INS, below), D, E, and g-values are indirectly determined through simulation of the HFEPR spectrum.

In INS, when an incident neutron beam hits a sample, the spins of neutrons and unpaired electrons in the sample interact, leading to the excitation of the sample from the ground M_S = ±3/2 state to the excited M_S = ±1/2 state. The energy difference between the incoming and outgoing neutrons was measured, giving the energy of the excited state, i.e., 2D'. The incident neutron beam may also lead to vibrational excitations of atoms, giving phonon peaks. In contrast to FIRMS, which relies on external magnetic fields of 0−17 T (and 5 K alone) to distinguish the magnetic peak from those of phonons, INS *may* not need a magnetic field to reveal the magnetic peak. Instead, variable-temperature (VT) INS spectra in the current work are analyzed to identify the magnetic peak from the excitation of the unpaired electrons (spin = 1/2), which, as fermions, follow the Boltzmann distribution (or Maxwell−Boltzmann statistics). In contrast, phonons/vibrations (spin = 0) are bosons following Bose−Einstein statistics. Thus, magnetic and phonon peaks show different temperature profiles, which are used to identify the magnetic peak. DFT phonon calculations give phonon energies, their symmetries, and a calculated *phonon* INS spectrum. Comparison between the experimental INS spectra, which have both magnetic and phonon peaks, and the calculated INS *phonon* spectrum helps identify the magnetic peak in the experimental spectra. Neutron scattering for coordination chemistry research, including features of different neutron instruments, has been discussed recently.[94]

Figure 3-top shows far-IR spectra of **Re−I** at 0 and 17 T. In the spectrum at 0 T, the smoothly rising baseline from the instrument is superimposed by several absorption dips from the sample. Among these dips, one corresponds to the absorption from the zero-field transition (from the ground M_S = ±3/2 state to the excited M_S = ±1/2 state). A comparison of the spectra at 0 and 17 T reveals slight mismatches in the dips due to the Zeeman effect. To highlight these changes, the transmission at each magnetic field is normalized by dividing it by the average transmission across all fields. The result is presented as an energy vs. magnetic field plot (also known as a heatmap) in Figure 3-bottom. One feature at 28.3(5) cm^{-1} exhibits a significant shift to higher energy. This behavior, along with the absence of the corresponding absorption dip in the 17 T spectrum (Figure 3-Top), suggests that it is from the M_S = ±3/2 → ±1/2 transition at 0 T or 2D' = 28.3(5) cm^{-1}.

The HFEPR spectrum of **Re−I** at 68 GHz (2.3 cm^{-1}) in Figure 4 is consistent with the $\phi_1 \rightarrow \phi_2$ transition (Figure 1). The spectra at different fields are simulated with $|D|$ = 13.1 cm^{-1}, $|E|$ = 3.02 cm^{-1} ($|E/D|$ = 0.23) for two cases: D > 0 (red trace) and D < 0 (blue trace), with g = [1.9, 1.9, 1.8]. The experimental spectra align well when D is negative. The SH parameters from HFEPR (Table 2) are used to simulate the changes in the FIRMS heat map (Figure 3-bottom) using *EasySpin*, giving colored lines in the plot that show good agreement between FIRMS and HFEPR. The lines represent so-called turning points[95] along the x, y, and z directions of the D tensor.

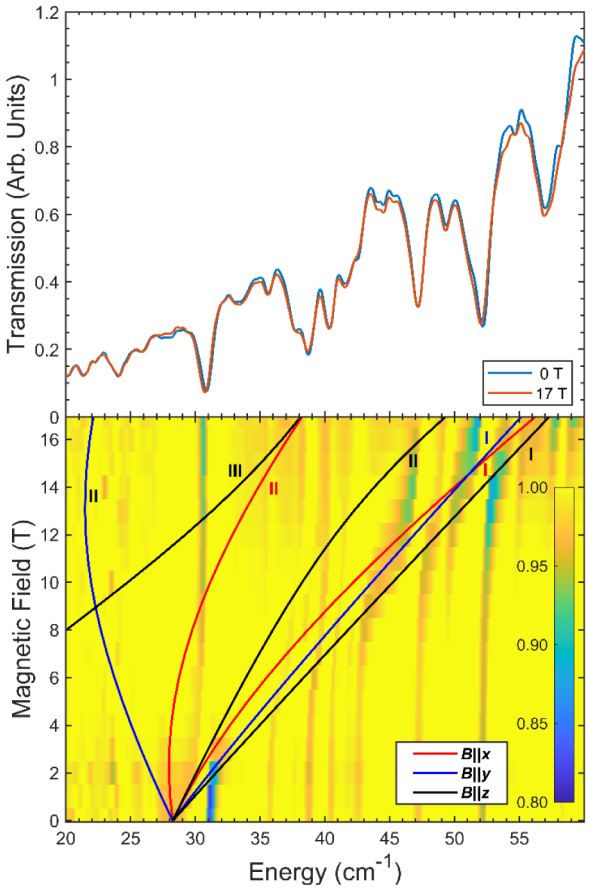


Figure 3. (Top) Far-IR transmission spectra of **Re−I** at 5.5 K for 0 and 17 T. (Bottom) FIRMS heat map, revealing the M_S = ±3/2 → ±1/2 transition and 2D' = 28.3(5) cm^{-1}, and the evolution of this transition under magnetic field. Red, blue, and black lines are results of *EasySpin* simulations using the SH parameters determined experimentally by FIRMS and HFEPR: D = −13.1 cm^{-1}, $|E|$ = 3.02 cm^{-1}, g = [1.9, 1.9, 1.8]. The I, II, and III labels are indicated in Figure 1. FIRMS results from another sample of **Re−I**, showing the magnetic transition, are given in Figure S6 in SI.

For INS spectra, VISION offers detectors for forward- and backscattered neutrons.[87,94] Forward-scattering detectors are associated with low Q (Q is the magnitude of the momentum-transfer $\boldsymbol{Q}$ vector[94]), while backscattering detectors are associated with high Q. Magnetic transitions are more pronounced in forward scattering at low Q.[94] The Bose correction to INS spectra highlights magnetic peaks by applying frequency- and temperature-dependent normalization to phonons that follow Bose−Einstein statistics.

The INS experiment was conducted without an external magnetic field, revealing directly the M_S = ±3/2 → ±1/2 transition (or ZFS = 2D') in Figure 1. VT, Bose-corrected INS spectra of **Re−I** in Figure 5 show a magnetic transition at 28 cm^{-1}. The signal-to-noise ratios for the peaks above 25 K are small. However, several features support its assignment as magnetic. This transition is more pronounced in the forward-scattering spectra than in the backscattering VT spectra in Figure S9-Top. This peak also increases in intensity as the temperature decreases because of the Boltzmann distribution of molecules in the two doublets (M_S = ±3/2, ±1/2), indicating that the peak is magnetic. For example, the intensity of the 28 cm^{-1} peak increases significantly from 125 to 5 K, while the intensities of other peaks do not show substantial

Downloaded from pubs.acs.org/inoca/article-pdf/65/41/24492/6737108/acs.inorgchem.6c04158.pdf by FLORIDA STATE UNIV user on 02 November 2026

https://doi.org/10.1021/acs.inorgchem.6c04158
Inorg. Chem. 2026, 65, 24492−24504

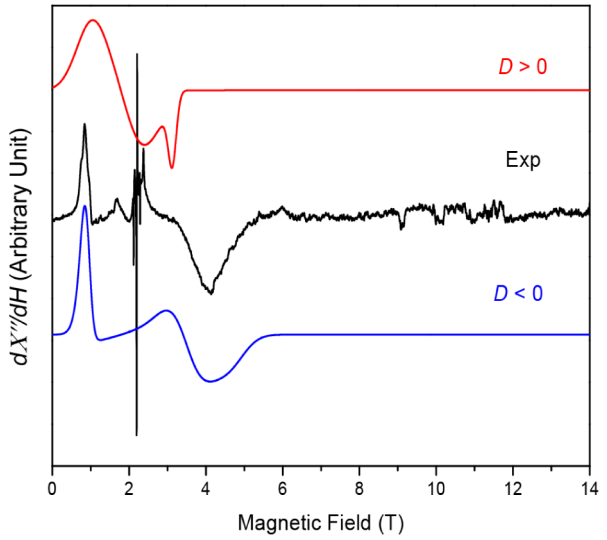


Figure 4. HFEPR spectrum (black trace) of **Re−I** powders at 5 K and 67 GHz, which is an average of crystallites in the *x*, *y*, and *z* directions. dX''/dH = first derivative of the absorption X″ vs *H*. The spectrum is simulated using $|D| = 13.1\ cm^{-1}$, $|E| = 3.02\ cm^{-1}$ ($|E/D| = 0.23$) for two cases: $D > 0$ (red trace) and $D < 0$ (blue trace), and $g = [1.9, 1.9, 1.8]$. The single-crystal line width used in the simulations was 0.1 T for the parallel turning point[95] and 0.4 T for the perpendicular turning points, with a 50:50 Gaussian/Lorentzian shape. Comparison of the simulated spectra with the experiment strongly suggests that $D < 0$. The narrow isotropic resonances over $g = 2.25–2.00$ belong to impurities.

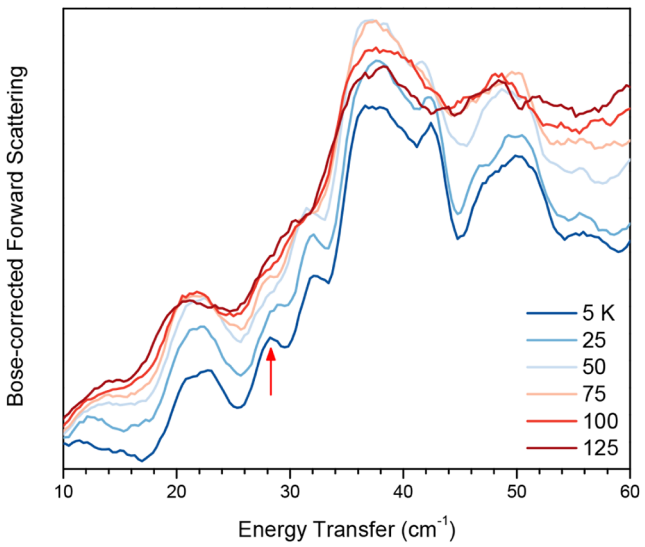


Figure 5. Bose-corrected, forward-scattering, VT INS spectra of **Re−I** at 0 T. The arrow points to the magnetic transition.

changes. Also, the calculated *phonon* spectrum (Figure S9-bottom) does not show this peak, supporting its magnetic origin. FIRMS of **Re−I** in Figures 3 and Figure S6 in SI discussed earlier, show the magnetic transition at 28.3(5) cm^{-1}.

FIRMS spectra of **Re−Br** and **Re−Cl** near the detection limit of ∼10 cm^{-1} of the far-IR spectrometer are given in Figure S7. Analyses of these spectra were not conclusive, as magnetic transitions most likely appear below the far-IR detection limit. In addition, the presence of three and four unique **Re−Br** and **Re−Cl** molecules in their respective crystallographic unit cells precluded the analysis of magnetic features (i.e., ZFS) in each unique molecule, as the FIRMS measurements yielded spectra averaged over the different molecules. Attempts to simulate HFEPR spectra of **Re−Cl** and **Re−Br** (Figure S8) were not successful. Most likely, the spectra are also complicated by the presence of multiple magnetically inequivalent centers. Additional discussion is given in the SI.

Magnetometry Studies

SH parameters may be determined from fitting DC magnetic susceptibility data, although the results are often erroneous. DC susceptibility data for **Re−X** were simulated using SH parameters obtained from spectroscopies (FIRMS, HFEPR, or INS) for **Re−I** or from *ab initio* calculations (see below) for the three complexes for comparison. AC susceptibilities are needed to determine whether a complex is an SMM and by which pathway its molecules relax from magnetically excited states. For **Re−Cl** and **Re−Br** complexes with multiple centers, the experimental magnetic susceptibility reflects an average of the contributions of centers.

DC magnetic molar susceptibility (χ_M) data were collected under an applied field of 0.1 T at 2−150 K (Figure 6). For each complex, the $\chi_M T$ maxima occur at 150 K and are approximately 1.54 (**Re−Cl**), 1.74 (**Re−Br**), and 1.40 (**Re−I**) $cm^3\ mol^{-1}\ K$. Comparing these values to $\chi_M T = 1.875$ for a typical $S = 3/2$ system suggests possible distributions of spin over the Re−X bonds and nonmetal atoms, especially X^- ions, in the molecules. This interpretation is supported by calculated spin densities in **Re−I** from VASP (*Vienna Ab initio Simulation Package*) calculations. In addition to providing phonon modes and energies for **Re−I** discussed below, the DFT calculations by VASP also provide spin densities for each atom in the molecule (Table S2), including 2.284 on the Re^{IV} ion, 0.218 on the six I^- ligands, and 0.028 on the C, H, and N atoms of $NBu^n{}_4^+$ cations with a sum of 2.530. For the $S = 3/2$ complex (with a spin density of 3), the remaining 0.47 density is expected to be distributed on chemical bonds in the molecule and mostly on the six Re−I bonds.

A simulation of the $\chi_M T$ vs *T* curves was performed using the *PHI* program by Chilton and coworkers,[96] yielding temperature-independent paramagnetism (TIP) coefficients of 0.0002 (**Re−Cl**), 0.0024 (**Re−Br**), and 0.0015 (**Re−I**) $cm^3\ mol^{-1}\ K$. These values are in agreement with data for $[Re^{IV}X_6]^{2-}$ complexes with different counterions.[15] The gradual drop of $\chi_M T$ below 100 K in all three complexes shows good agreement with computed nonzero *D* and *E* values. For **Re−Cl**, a reasonable agreement between the experimental and CASSCF-computed $\chi_M T$ was achieved. However, there are discrepancies for **Re−Br** and **Re−I**, probably due to mixing between $5d^3$ ligand-field multiplets and $5d^4$-ligand charge-transfer states, which decreases in energy from **Re−Cl** to **Re−Br** to **Re−I** and leads to an increase in Re−X bond covalency in this order, as discussed below. Even though the four unique $[ReCl_6]^{2-}$ sites in the **Re−Cl** unit cell have different geometric distortions (with *D* and *E* parameters varying in sign and magnitude), they do not induce drastic changes in $\chi_M T$. The simulated $\chi_M T$ plot for **Re−I** using spectroscopic SH parameters (Table 2) yields better agreement with the experimental curve than that using *ab initio*-calculated parameters (Figure 6, right).

Magnetic relaxation dynamics were probed by AC susceptibility studies at 1.8−3.0 K under a 0.15 T field. **Re−**

Downloaded from pubs.acs.org/inoca/article-pdf/65/41/24492/6737108/acs.inorgchem.6c04158.pdf by FLORIDA STATE UNIV user on 02 November 2026

https://doi.org/10.1021/acs.inorgchem.6c04158
Inorg. Chem. 2026, 65, 24492−24504

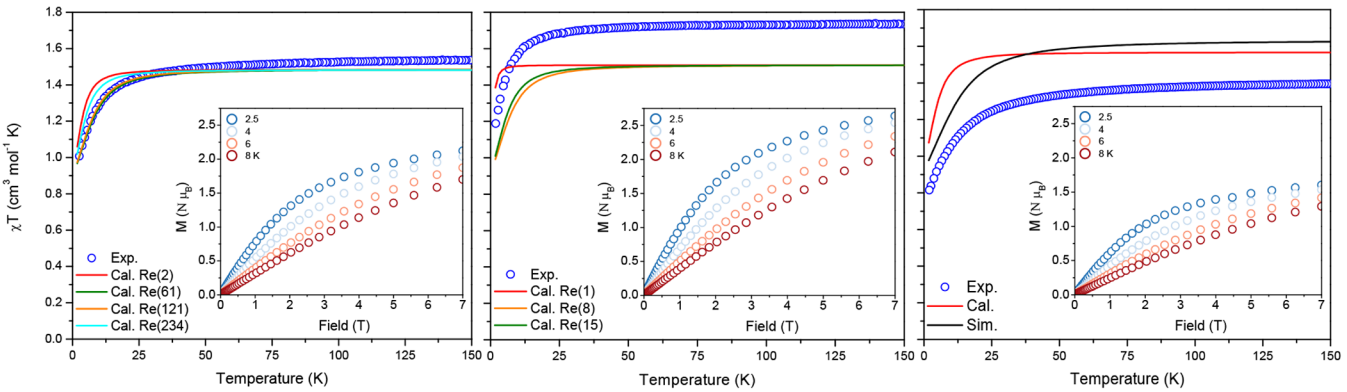


Figure 6. DC magnetic susceptibility at 0.1 T (Exp.) and values computed using spin-Hamiltonian parameters from CASSCF/NEVPT2 (Cal.) in Table 2: (Left) **Re−Cl**, (Middle) **Re−Br**, (Right) **Re−I**. For **Re−I**, simulated (Sim.) susceptibility was also calculated using spectroscopic SH parameters. Inset is the magnetization at 2.5, 4, 6, and 8 K.

I in Figure 7 displays a nonzero, out-of-phase AC signal (χ_M'') that gradually increases and shifts to lower frequencies as the

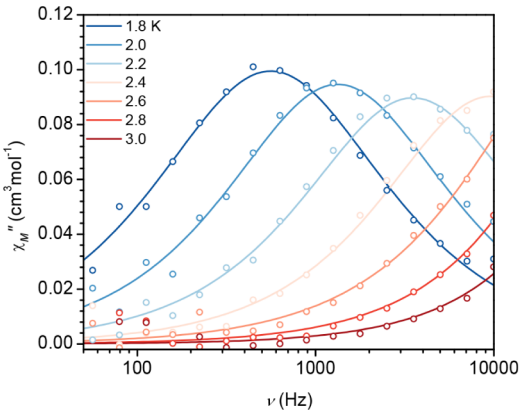


Figure 7. Frequency-dependent out-of-phase AC susceptibility at 1.8−3.0 K under a 0.15 T static DC field for **Re−I**.

temperature decreases, indicating that, upon lowering the temperature, magnetic relaxation slows down. **Re−Cl** (Figure S12-Top) and **Re−Br** (Figure S12-Middle) show high-frequency, nonzero, out-of-phase signals, but no maxima were observed up to 10 kHz. Therefore, analysis of the relaxation time for **Re−Cl** and **Re−Br** was not possible. Additional AC plots are provided in the SI.

The χ_M'' data of **Re−I** were processed by the *CC-FIT2* program to give τ and T values.[97] Three peaks were identified in Figure 7 and a fourth one was obtained through extrapolation. The relaxation data were fitted to the Raman mechanism in eq 2[98]

$$\tau^{-1} = CT^{n} \quad (2)$$

where C = constant for the Raman process; τ = relaxation time.

The ln τ vs ln T plot (Figure S14) gives $C = 8.9(4)$ s^{-1} and $n = 9.9(5)$ ($R^2 = 0.991$). For the Raman process, $n = 9$ is expected for Kramers ions. Cole−Cole plots (Figure S15) and discussions are given in the SI.

Studies of Spin-Phonon Couplings and Calculated Phonon Modes in Re−I

Spin-phonon coupling leads to magnetic relaxation[67,71] and therefore loss of memory in SMMs. The space group of **Re−I** is monoclinic $P2_1/n$ (No. 14) in the C_{2h} point group, giving phonons A_g, B_g, A_u, or B_u symmetry. The *u*-phonons are far-IR/FIRMS-active. We earlier studied spin-phonon couplings in $Co(acac)_2(H_2O)_2$[67] which crystallizes in the monoclinic $P2_1/c$ (No. 14) space group[99,100] in the C_{2h} point group. The Co^{II} ion in $Co(acac)_2(H_2O)_2$ is at the inversion center *i*, giving the molecule C_{2h} symmetry. In contrast, molecules of **Re−I** do not have the C_{2h} symmetry.

Spin-phonon couplings in **Re−I** are observed in FIRMS as avoided crossings between magnetic and phonon transitions. Through this coupling, the original magnetic and phonon transitions gradually hybridize, acquiring each other's character, as the field increases. Eventually, the magnetic transition becomes a phonon, while the phonon transition becomes magnetic, shifting to higher energy (to the right of the heat map in Figure 8). Figure 8 is reproduced from Figure 3-bottom to highlight spin-phonon couplings.

While spin-phonon couplings between magnetic and *u*-phonon transitions in **Re−I** have been probed by FIRMS,

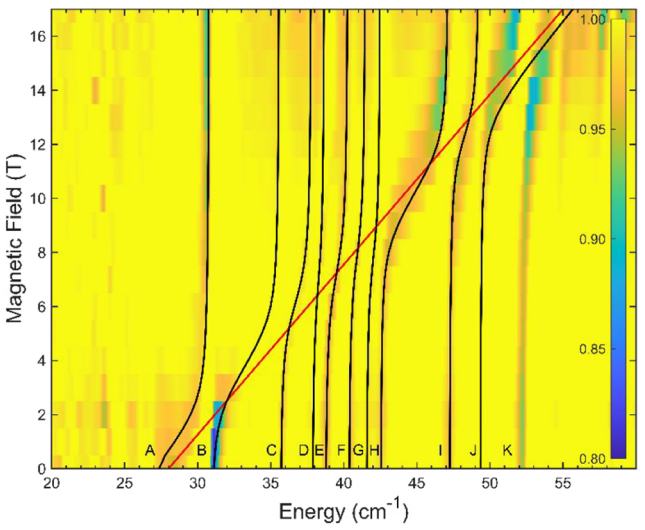


Figure 8. Fits to spin-phonon coupling in the **Re−I** FIRMS heat map using the *Maple* program.[101] Black solid lines are the fits for the magnetic peak (**A**) and phonon peaks (**B-J**). The red solid line is a linear fit for the approximate position of the magnetic transition between 0 and 17 T. At 0 T, peaks **A** and **B** likely undergo spin-phonon coupling, pushing peak **A** to the left. Phonon **K** was not included in the fit, as the 17 T field was not sufficient to observe its avoided crossing.

Downloaded from pubs.acs.org/inoca/article-pdf/65/41/24492/6873108/acs.inorgchem.6c04158.pdf by FLORIDA STATE UNIV user on 02 November 2026

https://doi.org/10.1021/acs.inorgchem.6c04158
Inorg. Chem. 2026, 65, 24492−24504

Table 3. Energies and Symmetries of Calculated Phonons in Re−I and Spin-Phonon Coupling Constants Λ

		A (sp)	B	C	D	E	F	G	H	I	J
Energy (cm^{-1})	FIRMS	28.3(5)	30.9(5)	35.6(5)	37.7(5)	38.7(5)	40.3(5)	41.6(5)	42.6(5)	47.2(5)	49.4(5)
	Cal'd		31.8	35.9	36.1	38.7	39.8	41.8	42.1	47.9	50.2
Λ_B-Λ_J (cm^{-1})			1.1(5)	1.0(5)	1.0(5)	1.0(5)	1.0(5)	1.0(5)	0.8(5)	1.0(5)	1.0(5)
Mode			A_u	B_u	A_u	A_u	B_u	B_u	A_u	B_u	B_u

phonon properties of the complex have been studied by INS. Unlike IR and Raman, which have different symmetry-based selection rules for phonon transitions, INS is a unique technique in which all phonon transitions are observable with *no* symmetry-based selection rules, as it is based on kinetic energy transfer between incident neutrons and the sample.[67,71] In addition, DFT phonon calculations with VASP provide an INS phonon spectrum, as well as the symmetries and energies of the phonon modes. The calculated phonon energies and their symmetries in **Re−I** are given in Table S3. Movies of selected calculated phonons near the magnetic transition are provided in the Supporting Information (SI), offering an opportunity to visualize the phonon motions.

Multiple phonons are observed to be involved in spin-phonon couplings. As magnetic transition **A** is blue-shifted (i.e., shifting to higher energy) with increasing magnetic field, it encounters phonon **B**. **B** progressively picks up the magnetic features, while **A** gradually becomes a phonon. This process is repeated with subsequent phonons. The coupling between the magnetic transition and each of the phonons can be simulated using the Hamiltonian in eq 3 consisting of the diagonal matrix elements of the expected energies of the spin (E_{sp}) and phonon (E_{ph}) excitations, along with the off-diagonal spin-phonon coupling energy (Λ):

$$H = \begin{pmatrix} E_{sp} & \Lambda \\ \Lambda & E_{ph} \end{pmatrix} \tag{3}$$

Diagonalizing the matrix gives two eigenvalues, $E_{\pm}$, producing the shift associated with the extent of interaction in eq 4:

$$\begin{vmatrix} E_{sp} - E_{\pm} & \Lambda \\ \Lambda & E_{ph} - E_{\pm} \end{vmatrix} = 0 \tag{4}$$

Expanding the model to 9 phonons, **B-J**, gives a 10 × 10 matrix (eq 5), assuming the phonon−phonon interactions (off-diagonal elements) are zero. Using eq 5 gives the fit in Figure 8 and the spin-phonon coupling constants Λ_B, Λ_C, ..., Λ_J in Table 3.

$$H = \begin{pmatrix} E_{sp} & \Lambda_B & \Lambda_C & \cdots & \Lambda_J \\ \Lambda_B & E_B & 0 & \cdots & 0 \\ \Lambda_C & 0 & E_C & \cdots & 0 \\ \vdots & \vdots & \vdots & \ddots & \vdots \\ \Lambda_J & 0 & 0 & \cdots & E_J \end{pmatrix} \tag{5}$$

Selected VASP-calculated phonon symmetries and energies of **Re−I** are given in Table 3. A full list of calculated phonon energies and symmetries is included in Table S3. The selected modes are those near the magnetic transition. All modes in this region are intermolecular in nature, involving long-range collective motion of atoms. "Wagging"/"twisting" are used to describe the local picture of the motions and should not be considered "intramolecular vibrations."

Phonon movies in the SI are provided to visualize the calculated modes. Vectors in the movies represent the magnitudes of the vibrations. The vibration amplitudes are scaled by a factor of 10 in the inset to highlight the motion at the metal center.

Phonon **B** at 31.8 cm^{-1} (A_u) is primarily C−H wagging of $NBu^n_4{}^+$ ions. The Bu^n groups show moderate counterclockwise cyclical twisting. Although the $[ReI_6]^{2-}$ motion is weak, a twisting motion is observed when enhanced in the movie. Phonon **C** at 35.9 cm^{-1} (B_u) is primarily the wagging of three Bu^n groups with moderate twisting of the fourth group. The $[ReI_6]^{2-}$ anion also undergoes a twisting motion. Phonon **D** at 36.1 cm^{-1} (A_u) is the omnidirectional wagging of Bu^n groups, leading to twisting of the $NBu^n_4{}^+$ unit, with $[ReI_6]^{2-}$ in a twisting motion. Phonon **E** at 38.7 cm^{-1} (A_u) is a wagging motion of both $NBu^n_4{}^+$ cations with moderate twisting in opposite directions. The $[ReI_6]^{2-}$ anion undergoes bending, as two *cis* I atoms move away from each other and the perpendicular **I** atoms bend toward them. Phonon **F** at 39.8 cm^{-1} (B_u) is similar in motion to phonon **C**, except that the twisting motion of the $NBu^n_4{}^+$ units is slightly different. Phonons **G** and **H** at 41.8 (B_u) and 42.1 cm^{-1} (A_u) show strong unidirectional wagging of the $NBu^n_4{}^+$ cations with twisting of the $[ReI_6]^{2-}$ anion. Phonons **I** and **J** at 47.9 (B_u) and 50.2 cm^{-1} (B_u) are similar in motion to phonon **E**, except that the C−H wagging motion is moderately different.

Vibrations around the first coordination sphere of $[ReI_6]^{2-}$ may have a greater impact on the structure, leading to magnetic relaxation. From the analysis of phonons **B-J**, two distinct motions about $[ReI_6]^{2-}$ are observed, independent of the overall phonon symmetry. Phonons **E**, **I**, and **J** exhibit bending motion, whereas other phonons exhibit twisting motion. No distinctive correlation has been identified between the symmetry or vibrational motion and the extent of spin-phonon coupling.

Re−X (X = Cl, Br, I) Bonding through the Eyes of Correlated Multireference Wavefunctions

To quantify and offer an insight into the chemical bonding in $[ReX_6]^{2-}$ from the perspective of ligand field theory, we have computed electronic energy levels derived from the $5d^3$ configurations. There are 10 S = 3/2 and 40 S = 1/2 electronic states spanned by these configurations. *Ab initio* ligand field theory (AILFT) allows us to extract the 5 × 5 matrices of the ligand field, the electron-repulsion (Racah) parameters B and C, and the spin-orbit coupling constant ζ. Separations between states having the maximum multiplicity are a function of the Racah parameter B,[102,103] which approximates the bond strength between the ligands and the metal ion. Racah parameter C indicates the energy difference between states of different multiplicity.[102,103] In $[ReX_6]^{2-}$, lone-pair electrons on the X^- ligands participate in π bonding to the metal ion. In such an octahedral ligand field, only one parameter, $10Dq$ (ligand-field splitting parameter, also called

Downloaded from pubs.acs.org/inoca/article-pdf/65/41/24492/6737108/acs.inorgchem.6c04158.pdf by FLORIDA STATE UNIV user on 02 November 2026

https://doi.org/10.1021/acs.inorgchem.6c04158
Inorg. Chem. 2026, 65, 24492−24504

Table 4. Ligand Field Parameters for $[ReX_6]^{2-}$ (X = Cl, Br, I) and the Re^{IV} Ion from *Ab Initio* Analyses of CASSCF/NEVPT2 of Wave Functions and Energy Eigenvalues

	$[ReCl_6]^{2-}$	$[ReBr_6]^{2-}$	$[ReI_6]^{2-}$	Re^{IV}
$10Dq$ (cm^{-1})	28702 [29000][a]	27144 [28000][a]	26112 [26000][a]	-
B (cm^{-1})	482 [442][a]	459 [414][a]	436 [404][a]	728
C (cm^{-1})	1765	1621	1353	3072
ζ (cm^{-1})	2652	2415	2055	3480
e_σ (cm^{-1})	16577	16099	16649	-
e_π (cm^{-1})	5278	5319	6016	-
D (cm^{-1})	−71	−64	−57	-
$\delta B\% = \left(\frac{B_{Re^{4+}} - B_{complex}}{B_{Re^{4+}}}\right) \times 100$	34	37	40	-
$\delta C\% = \left(\frac{C_{Re^{4+}} - C_{complex}}{C_{Re^{4+}}}\right) \times 100$	42	47	56	-
$\delta\zeta\% = \left(\frac{\zeta_{Re^{4+}} - \zeta_{complex}}{\zeta_{Re^{4+}}}\right) \times 100$	24	31	41	-

[a]Ref 1.

Δ_{oct}, as shown in Figure S1 in SI), given by the energy difference between the σ and π Re−X antibonding orbitals e_g* and t_{2g}*, respectively, governs the 5*d*-orbital splitting pattern and the energies of the multiplets. These parameters are listed in Table 4. Computed values of $10Dq$ compare well with reported data extracted from the spectra in Ref. 1. In Table 4, we also report parameters *B*, *C*, and ζ for an uncoordinated Re^{IV} ion. A decrease of these parameters in a complex is a measure of the covalency of the Re−halide bond, i.e., the so-called cloud-expansion (nephelauxetic) effect. Percentage reductions of *B*, *C*, and ζ as defined in Table 4 reflect an increase in the Re−X bond covalency from the lighter to the heavier ligands: Re−Cl < Re−Br < Re−I. For example, the reduction in *B* is 34% for the Re−Cl, 37% for the Re−Br, and 40% for the Re−I bonds. Compared with corresponding 3*d* Mn^{IV} complexes, covalency is greatly enhanced for the heavier Re^{IV}−X in comparison with the more ionic Mn^{IV}−X bonds.[104] Similar conclusions emerge from variations in *C* and in the spin-orbit coupling constant ζ. The reason for this dependence is the proximity of ligand-to-metal charge-transfer states, which mix intensively into the lower-lying states of $5d^3$ character. The nearly octahedral geometry of ReX_6^{2-} did not allow extraction of the angular overlap model parameters e_σ and e_π (which quantify the σ- and π-antibonding parameters), respectively, from the energies of molecular orbitals dominated by 5*d* atomic orbitals. To this end, we have carried out calculations on distorted complexes by applying a 3° compression of each ReX_6^{2-} octahedron along one of the four equivalent trigonal axes. By applying the same distortion to all three complexes, we were able to study the net effect of spin-orbit coupling on the magnetic anisotropy, quantified by *D*. The computed values *D* = −71, −64, and −57 cm^{-1} in Table 4 for $ReCl_6^{2-}$, $ReBr_6^{2-}$, and ReI_6^{2-}, respectively, reflect a decrease of the magnetic anisotropy across the series. Values of e_σ and e_π resulting from such analysis are also included in Table 4. High e_σ values of 16577, 16099, and 16649 cm^{-1} for the Re−Cl, Re−Br, and Re−I bonds, respectively, do not show a monotonic trend within the triad. This most probably reflects the increase in the Re−X bond distance from **Re−Cl** to **Re−Br** (correlating with a lowering of e_σ) which is overcompensated by more diffuse and better-overlapping ligand orbitals in the case of **Re−I.** In contrast, e_π increases monotonically across the series from Cl^- to Br^- to I^-, thus reflecting the corresponding increase in Re−X bond covalency.

We have also carried out electronic structure calculations on **Re−I** after extending the active space from the traditional CAS(3,5) (three electrons distributed over the five 3*d* molecular orbitals) to CAS(13,10) (having the three electrons and their bonding partners—the five bonding molecular orbitals occupied by two electrons each, which establish the chemical bonding in the complex). This resulted in a 3 + 2 × 5 = 13 electrons over 5 + 5 = 10 orbitals model space for CASSCF. However, these calculations did not result in a negative value for *D*. The positive value 5−6 cm^{-1} came as a stable result.

A possible reason for the discrepancy is that I-to-Re charge transfer is very low-lying in energy because of strong mixing between I^- and Re^{IV} orbitals. Thus, the d^3 configuration is relatively ill-defined. In such a case, even the extended CAS(13,10) active space is still not enough to capture the strong Re−I bond covalency. Furthermore, the possibility of a temperature-dependent structural change was ruled out by the observation of no significant differences in the powder neutron diffraction (PND) between 5 and 100 K, as shown in Figure S3.

Whether the heavy-atom effect contributes to ZFS in **Re−X** has been considered. Spin-orbit coupling (SOC) constants for Cl, Br, and I atoms were computed in a model in which closed-shell Cl^-, Br^- and I^- ions have lost one of the *p*-electrons in the excited ligand-to-metal charge-transfer configuration, leading to Cl, Br, and I atoms with one hole in the $2p^5$ shell in a ^2P ground state. The CAS(5,3) active space was used to compute the $^2P_{J=1/2}$ and $^2P_{J=3/2}$ states, showing that the energy separation $E(^2P_{J=1/2}) - E(^2P_{J=3/2})$ is just $-(3/2)\zeta$, where ζ is the SOC constant. The resulting ζ values for the Cl, Br, and I atoms are −574 cm^{-1}, −2243 cm^{-1}, and −4689 cm^{-1}, respectively. The results on the halogen X atoms here suggest the following: (1) The negative ζ values imply that $J = 3/2$ is below $J = 1/2$ for the X atoms, which is also expected for the more-than-half-filled p^5 ground-state configurations of the

https://doi.org/10.1021/acs.inorgchem.6c04158
Inorg. Chem. 2026, 65, 24492−24504

Downloaded from pubs.acs.org/inoaj/article-pdf/65/41/24492/6737108/acs.inorgchem.6c04158.pdf by FLORIDA STATE UNIV user on 02 November 2026

halogen X atoms. (2) SOC dramatically increases from the lighter Cl atom to the heavier I atom. The SOC ζ value for the free Re^{IV} ion, in comparison, is +3480 cm^{-1} (Table 4). Here, the $J = 3/2$ ground state is below the $J = 5/2$ excited state for the Re^{IV} ion, and ζ is positive, as expected for a $5d^3$ ion that is less than half-filled.

If the heavy-ligand effect of the six halide ligands is present in the ReX_6^{2-} complexes, SOC in the X^- ligands would add constructively to that of the free Re^{IV} ion. In other words, the SOC values in the ReX_6^{2-} complexes are expected to increase from **Re−Cl Re−Br**, to **Re−I**. However, calculations [Table 4, fourth row: ζ = 2652 cm^{-1} ($ReCl_6^{2-}$), 2415 cm^{-1} ($ReBr_6^{2-}$), 2055 cm^{-1} (ReI_6^{2-}), 3480 cm^{-1} (free Re^{IV} ion)] show that the trend is just the opposite. This is consistent with the values of D (Table 4 and the above discussion), which show a decrease in magnetic anisotropy in the same order. The results indicate that, upon formation of Re−X bonds in the complexes, SOC effects of the Cl, Br, and I atoms subtract from that of Re^{IV}. Such behavior was also reported for a series of tetrahedral Ni^{II} complexes, showing a vanishingly small ζ value in the case of NiI_4^{2-}.[105] The decrease in the ζ values from **Re−Cl**, **Re−Br**, to **Re−I** in our calculations suggests that there is no heavy-atom effect of the halogen atoms here. The current work is a rare study of the heavy-atom effect on ZFS, especially for SMMs.[66] The results here suggest that the structures of the complexes and ligands are more important contributors to ZFS (and to the potential barriers for spin reversal in SMMs) than the heavy atoms of the ligands.

CONCLUSION

This is a comprehensive study of structures, magnetic anisotropy, phonons, spin-phonon coupling, and magnetic relaxation in transition-metal complexes using multiple state-of-the-art techniques as well as advanced *ab initio* analyses and DFT phonon calculations. Distortion from O_h in $(NBu^n_4)_2[ReX_6]$ (**Re−Cl**, **Re−Br**, **Re−I**) leads to magnetic anisotropy, and the covalency of the Re−X bond influences the anisotropy. Advanced spectroscopies (FIRMS, HFEPR, and INS) enable the determination of SH parameters for **Re−I** that agree well with DC susceptibility data. There is a significant drop in SMM performance from **Re−I** to **Re−Cl** and **Re−Br**. This performance is reflected by the large, negative D in **Re−I**, whereas the D values in **Re−Cl** and **Re−Br** are relatively small and variable in sign. **Re−Cl** and **Re−Br** have multiple inequivalent metal centers that may contribute to a decrease in SMM performance. Spin-phonon couplings were probed by examining phonons near the magnetic transition, which may lead to a dominant Raman-mediated relaxation in **Re−I**. *Ab initio* analyses extracted ligand-field parameters showing large SOC and an increase in covalency from **Re−Cl** to **Re−Br** to **Re−I**.

EXPERIMENTAL SECTION

All reagents were received from commercial sources and used without further purification unless otherwise specified. Potassium perrhenate ($KReO_4$, 99%) and hydroiodic acid (HI, 57%, stabilized with 1.5% hypophosphorous acid) were purchased from Alfa Aesar. KX salts were purchased from Mallinckrodt. Concentrated HCl and HBr were purchased from Fisher Scientific. Tetrabutylammonium hydroxide (NBu^n_4OH, 55% in water) was purchased from Oakwood Chemicals.

Syntheses of Re−X

$(NBu^n_4)_2[ReX_6]$ (**Re−Cl**, **Re−Br**, **Re−I**) were prepared according to literature methods, with slight modifications.[55,106] $KReO_4$ (1.0 g, 3.5 mmol) and KX [X = Cl (0.26 g), Br (0.42 g), I (0.58 g), 3.5 mmol] were combined in 10 mL of concentrated HX, followed by gentle boiling for 2 h. The solvent was reduced by heating, and the concentrated solution was cooled to room temperature and then chilled in an ice bath. The solid product (K_2ReX_6) was then extracted from the solution by vacuum filtration using a glass-fritted funnel in yields of 58−78%. Paper filtration is not advised, as concentrated acids decompose the filters. Metathesis of K_2ReX_6 [X = Cl (1.0 g), Br (1.5 g), I (2.1 g), 2.0 mmol] with excess NBu^n_4OH (>4 mmol) in aqueous 0.1 M HX solution at room temperature gives precipitates, which are collected by filtration, washed with water, and dried with Et_2O in yields of 74−92%. A minimal amount of insoluble black solid, which is metallic Re, sometimes forms during the reaction. This solid was removed by dissolving the mixture in acetone and collecting the filtrate.

For $(NBu^n_4)_2[ReI_6]$ (**Re−I**), an alternative synthesis was performed by combining K_2ReI_6 and NBu^n_4I in a 1:2 molar ratio in acetone, stirring for 2 h at room temperature, and then adding hexanes to precipitate the product. This alternative procedure was later used to minimize decomposition of **Re−I**, which was found to decompose over time.

Single-Crystal X-ray Diffraction

Suitable single crystals of **Re−Cl**, **Re−Br** and **Re−I** were coated in Paratone oil and mounted on a MiTeGen loop under a cold stream of nitrogen (100 K). Single-crystal X-ray diffraction data were collected using a Bruker D8 Venture diffractometer with a PHOTON 100 detector (Mo K_α radiation, λ = 0.71073 Å). Frames were collected with the APEX2 program and reduced using the Bruker SAINT software, with absorption correction by the SADABS multiscan program. Structures of **Re−Cl**, **Re−Br** and **Re−I** were solved with SHELXS and refined with SHELXL-2014. The CIF files of the single-crystal structures are available from the Cambridge Crystallographic Data Centre (CCDC): Deposition Nos. 2348938 (**Re−Cl**), 2348939 (**Re−Br**), and 2348940 (**Re−I**).

Details of DC/AC magnetometry measurements, FIRMS, HFEPR, and INS, as well as phonon and INS calculations, are given in the SI.

Ab Initio Calculations of Spectroscopic and Magnetic Properties and Bonding Analysis

Calculations of scalar-relativistic energies and wavefunctions were carried out with the ORCA package[107−109] using coordinates obtained from the X-ray crystallographic data. Many-particle wavefunctions and energy eigenvalues of electronic states spanned by the $5d^3$ configuration of Re^{IV} were computed using the state-averaged complete active space self-consistent field method (SA-CASSCF).[110−112] To account for dynamical correlation, we have used the n-electron valence perturbation theory to second order (NEVPT2).[113−115] Scalar relativistic effects were incorporated, employing the Douglas-Kroll-Hess (DKH) approximation.[116] Here, we have employed the DKH-adapted version of the def2-TZVP basis set for Re, Cl, Br, N, C, and H atoms.[117,118] The DKH-adapted version of the Sapporo basis set was employed for the I atom.[119] *Ab initio* ligand field theory (AILFT) analyses were performed to examine the *d*-orbital ligand field splitting pattern.[73,104,120] To further quantify the nature of the Re-X bond, 5 × 5 one-electron ligand-field matrices were fitted with e_σ and e_π parameters defined in the Angular Overlap Model (AOM).

ASSOCIATED CONTENT

Supporting Information

The Supporting Information is available free of charge at https://pubs.acs.org/doi/10.1021/acs.inorgchem.6c04158.

Movies of VASP-calculated phonons of **Re−I** in the 28.76−52.81 cm^{-1} range (ZIP)

Author contributions, additional experimental section, partial MO diagram in $[ReX_6]^{2-}$ and ZFS in the D_{4h} crystal field, single-crystal X-ray, powder X-ray, and neutron diffraction, IR spectra of the samples, additional

Downloaded from pubs.acs.org/inoca/article-pdf/65/41/24492/6737108/acs.inorgchem.6c04158.pdf by FLORIDA STATE UNIV user on 02 November 2026

https://doi.org/10.1021/acs.inorgchem.6c04158
Inorg. Chem. 2026, 65, 24492−24504

FIRMS, HFEPR, INS results, additional magnetic susceptibility data, calculated spin densities in **Re−I**, calculated phonon modes in **Re−I** and their symmetries, distortion of $[ReX_6]^{2-}$ analyzed by *SHAPE*, and input for ORCA calculations (PDF)

Accession Codes

Deposition numbers 2348938−2348940 contain the supplementary crystallographic data for this paper. These data can be obtained free of charge via the joint Cambridge Crystallographic Data Centre (CCDC) and Fachinformationszentrum Karlsruhe Access Structures service.

AUTHOR INFORMATION

Corresponding Authors

Mihail Atanasov − *Max-Planck Institut für Kohlenforschung, Mülheim an der Ruhr 45470, Germany; Institute of General and Inorganic Chemistry, Bulgarian Academy of Sciences, Sofia 1113, Bulgaria;* orcid.org/0000-0003-4178-2187; Email: mihail.atanasov@kofo.mpg.de

Zi-Ling Xue − *Department of Chemistry, University of Tennessee, Knoxville, Tennessee 37996, United States;* orcid.org/0000-0001-7401-9933; Email: xue@utk.edu

Authors

Adam T. Hand − *Department of Chemistry, University of Tennessee, Knoxville, Tennessee 37996, United States*

Alexandria N. Bone − *Department of Chemistry, University of Tennessee, Knoxville, Tennessee 37996, United States*

Shashank V. Rao − *Max-Planck Institut für Kohlenforschung, Mülheim an der Ruhr 45470, Germany;* orcid.org/0000-0002-0152-360X

Brandon D. Watson-Sanders − *Department of Chemistry, University of Tennessee, Knoxville, Tennessee 37996, United States;* orcid.org/0000-0002-9276-9508

Adiat A. Fakolujo − *Department of Chemistry, University of Tennessee, Knoxville, Tennessee 37996, United States;* orcid.org/0009-0007-1742-5426

Yongqiang Cheng − *Neutron Scattering Division, Oak Ridge National Laboratory, Oak Ridge, Tennessee 37831, United States;* orcid.org/0000-0002-3263-4812

Mykhaylo Ozerov − *National High Magnetic Field Laboratory, Florida State University, Tallahassee, Florida 32310, United States;* orcid.org/0000-0002-5470-1158

J. Krzystek − *National High Magnetic Field Laboratory, Florida State University, Tallahassee, Florida 32310, United States;* orcid.org/0000-0001-6088-1936

Zheng Gai − *Center for Nanophase Materials Sciences, Oak Ridge National Laboratory, Oak Ridge, Tennessee 37831, United States;* orcid.org/0000-0002-6099-4559

Wei Lv − *State Key Laboratory of Coordination Chemistry, School of Chemistry, Nanjing University, Nanjing 210023, China*

Xue-Tai Chen − *State Key Laboratory of Coordination Chemistry, School of Chemistry, Nanjing University, Nanjing 210023, China;* orcid.org/0000-0001-5518-5557

You Song − *State Key Laboratory of Coordination Chemistry, School of Chemistry, Nanjing University, Nanjing 210023, China;* orcid.org/0000-0002-0289-7830

Luke L. Daemen − *Neutron Scattering Division, Oak Ridge National Laboratory, Oak Ridge, Tennessee 37831, United States*

Xiaoping Wang − *Neutron Scattering Division, Oak Ridge National Laboratory, Oak Ridge, Tennessee 37831, United States;* orcid.org/0000-0001-7143-8112

Frank Neese − *Max-Planck Institut für Kohlenforschung, Mülheim an der Ruhr 45470, Germany;* orcid.org/0000-0003-4691-0547

Complete contact information is available at: https://pubs.acs.org/10.1021/acs.inorgchem.6c04158

Notes

The authors declare no competing financial interest.

ACKNOWLEDGMENTS

The U.S. National Science Foundation [CHE-2349345 to Z.-L.X. and DGE-2152168 for NRT (Research Traineeship Program) fellowships to A.T.H. and B.D.W.S.] supported the research at the University of Tennessee. The National Natural Science Foundation of China (22373048 to Y.S.) sponsored the work at Nanjing University. Both DC and AC magnetic property studies were conducted in part at the Center for Nanophase Materials Sciences at Oak Ridge National Laboratory, which is sponsored by the Scientific User Facilities Division, Office of Basic Energy Sciences, U.S. Department of Energy. AC susceptibility data (10,000 Hz) were collected on the PPMS at the State Key Laboratory of Coordination Chemistry, School of Chemistry and Chemical Engineering, Nanjing University. We thank Dr. Tianwei Wang for help with the AC (10,000 Hz) measurements, Dr. Phattananawee Nalaoh and Michael J. Jenkins for help with the determination of the crystal structure of **Re−I**, and Dr. A. Ozarowski for the EPR software package SPIN. Part of this work was performed at the National High Magnetic Field Laboratory, which is supported by NSF Cooperative Agreement No. DMR-2128556 and the State of Florida. Neutron scattering experiments were conducted at the VISION beamline at ORNL's Spallation Neutron Source, which is supported by the Scientific User Facilities Division, Office of Basic Energy Sciences (BES), U.S. Department of Energy (DOE), under Contract No. DE-AC05-00OR22725 with UT-Battelle, LLC. The computing resources were made available through the VirtuES and ICEMAN projects, funded by the Laboratory Directed Research and Development program and the Compute and Data Environment for Science (CADES) at ORNL; Mihail Atanasov, Shashank Vital Rao, and Frank Neese thank the Max Planck Society for financial support of this work.

REFERENCES

(1) Jørgensen, C. K.; Schwochau, K. Comparative Interpretation of Absorption Spectra of Technetium(IV) and Rhenium(IV) Hexahalides. *Z. Naturforsch., A* **1965**, *20*, 65−75.

(2) Pross, L.; Rössler, K.; Schenk, H. J. Optical studies on crystalline hexahalorhenates—I: Low temperature absorption spectra of $K_2[ReCl_6]$ single crystals. *J. Inorg. Nucl. Chem* **1974**, *36*, 317−322.

(3) LoMenzo, J. A.; Strobridge, S.; Patterson, H. H.; Engstrom, H. Electronic absorption spectra of the $5d^3$ hexafluororhenate(IV) ion. *J. Mol. Spectrosc* **1977**, *66*, 150−161.

(4) Chatterjee, I.; Desai, V. P. Magnetic susceptibilities of antiferromagnetic Re^{4+} compounds. *Phys. Rev. B* **1981**, *24*, 5133−5138.

(5) Schoenen, N.; Schmidtke, H.-H. Low symmetry distortions of hexahalo anions of Re(IV) and Os(IV) investigated by polarized absorption spectra and ligand field calculations. *Mol. Phys* **1986**, *57*, 983−1004.

Downloaded from pubs.acs.org/inoca/article-pdf/65/41/24492/6737108/acs.inorgchem.6c04158.pdf by FLORIDA STATE UNIV user on 02 November 2026

(6) Tomkiewicz, A.; Villain, F.; Mrozinski, J. Magnetic properties and EXAFS study of methylammonium hexaiodorhenate(IV) salts. *J. Mol. Struct* **2000**, *555*, 383−390.
(7) González, R.; Chiozzone, R.; Kremer, C.; Guerra, F.; De Munno, G.; Lloret, F.; Julve, M.; Faus, J. Magnetic Studies on Hexahalorhenate(IV) Salts of Ferrocenium Cations $[Fe(C_5R_5)_2]_2[ReX_6]$ (R = H, CH_3; X = Cl, Br, I). *Inorg. Chem.* **2004**, *43*, 3013−3019.
(8) Balasekaran, S. M.; Molski, M.; Spandl, J.; Hagenbach, A.; Alberto, R.; Abram, U. Hexafluoridotechnetate(IV) Revisited. *Inorg. Chem* **2013**, *52*, 7094−7099.
(9) Gong, D.-P.; Chen, J.-F.; Zhao, Y.; Cao, D.-K. Bisthienylethene Th_2im and its complex $(Th_2imH)_2[ReCl_6]$: Crystalline-phase photochromism, and photochemical regulation of luminescence and magnetic properties. *Dalton Trans* **2016**, *45*, 3443−3449.
(10) Armentano, D.; Barquero, M. A.; Rojas-Dotti, C.; Moliner, N.; De Munno, G.; Brechin, E. K.; Martínez-Lillo, J. Enhancement of Intermolecular Magnetic Exchange through Halogen···Halogen Interactions in Bisadeninium Rhenium(IV) Salts. *Cryst. Growth Des* **2017**, *17*, 5342−5348.
(11) Haase, P. A. B.; Repisky, M.; Komorovsky, S.; Bendix, J.; Sauer, S. P. A. Relativistic DFT Calculations of Hyperfine Coupling Constants in 5*d* Hexafluorido Complexes: $[ReF_6]^{2-}$ and $[IrF_6]^{2-}$. *Chem. Eur. J* **2018**, *24*, 5124−5133.
(12) Poineau, F.; Louis-Jean, J.; Jang, H.; Higgins, C.; Balasekaran, S. M.; Hatchett, D.; Sattelberger, A. P. X-ray absorption fine structure spectroscopic study of $(NH_4)_2ReF_6$. *SN Appl. Sci* **2019**, *1*, 1442.
(13) Asanov, I. P.; Fedorenko, A. D.; Berdyugin, S. N.; Gaas, V. A.; Bogomyakov, A. S. Magnetic Properties of $(NH_4)_2[ReCl_6]$, $[Pd(NH_3)_4][ReCl_6]$, and $[Pt(NH_3)_4][ReCl_6]$ Compounds and the X-Ray Photoelectron Analysis of Their Electronic Structures. *J. Struct. Chem* **2026**, *67*, 632−643.
(14) Pedersen, K. S.; Sigrist, M.; Sørensen, M. A.; Barra, A.-L.; Weyhermüller, T.; Piligkos, S.; Thuesen, C. A.; Vinum, M. G.; Mutka, H.; Weihe, H.; et al. $[ReF_6]^{2-}$: A Robust Module for the Design of Molecule-Based Magnetic Materials. *Angew. Chem. Int. Ed.* **2014**, *53*, 1351−1354.
(15) Rojas-Dotti, C.; Sanchis-Perucho, A.; Orts-Arroyo, M.; Moliner, N.; Gonzalez, R.; Lloret, F.; Martinez-Lillo, J. Field-Induced Single-Ion Magnet Phenomenon in Hexabromo- and Hexaiodorhenate(IV) Complexes. *Magnetochemistry* **2020**, *6*, 20.
(16) Sanchis-Perucho, A.; Orts-Arroyo, M.; Camús-Hernández, J.; Rojas-Dotti, C.; Escrivà, E.; Lloret, F.; Martínez-Lillo, J. Hexahalorhenate(IV) salts of protonated ciprofloxacin: Antibiotic-based single-ion magnets. *CrystEngcomm* **2021**, *23*, 8579−8587.
(17) Louis-Jean, J.; Balasekaran, S. M.; Lawler, K. V.; Sanchis-Perucho, A.; Martínez-Lillo, J.; Smith, D.; Forster, P. M.; Salamat, A.; Poineau, F. Coexistence of metamagnetism and slow relaxation of magnetization in ammonium hexafluoridorhenate. *RSC Adv* **2021**, *11*, 6353−6360.
(18) Louis-Jean, J.; Forster, P. M.; Balasekaran, S. M.; Pham, C. T.; Poineau, F. Structural and spectral studies of hydrated hexaamminecobalt(III)−hexafluororhenate(IV). *J. Fluorine Chem* **2021**, *252*, 109903.
(19) Taran, L. S.; Elfimova, V. Y.; Streltsov, S. V. Magnetic Anisotropy of Single-Ion Magnet $(PPh_4)_2[ReF_6]\cdot 2H_2O$. *JETP Lett* **2023**, *117*, 606−611.
(20) Vyaselev, O. M.; Kushch, N. D.; Yagubskii, E. B.; Maximova, O. V.; Vasiliev, A. N. Spin dynamics in two $[ReF_6]$-based single-molecule magnets from NMR and ac susceptibility measurements. *Phys. Rev. B* **2020**, *101*, 134427.
(21) Piccinelli, F.; Bettinelli, M.; Cano, J.; Lloret, F.; Julve, M.; Dolmella, A. Magnetic Properties of a New Hexahalorhenate(IV) Compound and Structural Comparison with Its Hexahaloplatinate-(IV) Analog. *Eur. J. Inorg. Chem* **2020**, *2020*, 2246−2252.
(22) Liu, J.-L.; Pedersen, K. S.; Greer, S. M.; Oyarzabal, I.; Mondal, A.; Hill, S.; Wilhelm, F.; Rogalev, A.; Tressaud, A.; Durand, E.; et al. Access to Heteroleptic Fluorido-Cyanido Complexes with a Large Magnetic Anisotropy by Fluoride Abstraction. *Angew. Chem. Int. Ed.* **2020**, *59*, 10306−10310.
(23) Singh, S. K.; Rajaraman, G. Deciphering the origin of giant magnetic anisotropy and fast quantum tunnelling in rhenium(IV) single-molecule magnets. *Nat. Commun* **2016**, *7*, 10669.
(24) Gryca, I.; Palion-Gazda, J.; Machura, B.; Penkala, M.; Kruszyński, R.; Cano, J.; Lloret, F.; Julve, M. Synthesis, crystal structure and magnetic properties of H_2tppz$[ReCl_6]$ and $[Cu(bpzm)_2(\mu\text{-Cl})ReCl_3(\mu\text{-ox})Cu(bpzm)_2(\mu\text{-ox})ReCl_3(\mu\text{-Cl})]_n$. *Dalton Trans* **2015**, *44*, 17118−17128.
(25) Ferrari-Argachá, C.; Valiero, S.; Rojas-Dotti, C.; Loaces, A.; Chiozzone, R.; Moliner, N.; Suescun, L.; Cano, J.; Lloret, F.; Martínez-Lillo, J.; et al. Self-assembly of lanthanide-based single-ion magnets (SIMs) into 1D networks via Re(IV)-based metalloligands. *Dalton Trans.* **2026**, *55*, 854−864.
(26) Bar, A. K.; Pichon, C.; Sutter, J.-P. Magnetic Anisotropy in Two- to Eight-Coordinated Transition-Metal Complexes: Recent Developments in Molecular Magnetism. *Coord. Chem. Rev* **2016**, *308*, 346−380.
(27) Benelli, C.; Gatteschi, D. *Introduction to Molecular Magnetism: From Transition Metals to Lanthanides*; Wiley-VCH, 2015.
(28) Andres, H.; Basler, R.; Güdel, H.-U.; Aromí, G.; Christou, G.; Büttner, H.; Rufflé, B. Inelastic neutron scattering and magnetic susceptibilities of the single-molecule magnets $[Mn_4O_3X(OAc)_3(dbm)_3]$ (X = Br, Cl, OAc, and F): Variation of the anisotropy along the series. *J. Am. Chem. Soc* **2000**, *122*, 12469−12477.
(29) Feng, M.; Tong, M.-L. Single Ion Magnets from 3*d* to 5*f*: Developments and Strategies. *Chem. Eur. J* **2018**, *24*, 7574−7594.
(30) Figgis, B. N.; Lewis, J.; Mabbs, F. E. The Magnetic Properties of Some d^3-complexes. *J. Chem. Soc* **1961**, 3138−3145.
(31) Frost, J. M.; Harriman, K. L. M.; Murugesu, M. The rise of 3*d* single-ion magnets in molecular magnetism: towards materials from molecules? *Chem. Sci* **2016**, *7*, 2470−2491.
(32) Gao, S. *Molecular Nanomagnets and Related Phenomena*; Springer, 2015.
(33) Gatteschi, D.; Sessoli, R.; Villain, J. *Molecular Nanomagnets*; Oxford University Press, 2006.
(34) Gomez-Coca, S.; Urtizberea, A.; Cremades, E.; Alonso, P. J.; Camon, A.; Ruiz, E.; Luis, F. Origin of Slow Magnetic Relaxation in Kramers Ions with Non-uniaxial Anisotropy. *Nat. Commun* **2014**, *5*, 4300.
(35) Holynska, M. *Single-Molecule Magnets: molecular Architectures and Building Blocks for Spintronics*; Wiley-VCH, 2019.
(36) Liddle, S. T.; van Slageren, J. Improving *f*-element Single Molecule Magnets. *Chem. Soc. Rev* **2015**, *44*, 6655−6669.
(37) Lu, J.; Guo, M.; Tang, J. Recent Developments in Lanthanide Single-Molecule Magnets. *Chem. Asian J* **2017**, *12*, 2772−2779.
(38) McInnes, E. J. L.; Winpenny, R. E. P.Molecular Magnets *Comprehensive Inorganic Chemistry II*. Poeppelmeier, K. Ed.; Elsevier, 2013
(39) Sarkar, A.; Dey, S.; Rajaraman, G. Role of Coordination Number and Geometry in Controlling the Magnetic Anisotropy in Fe^{II}, Co^{II}, and Ni^{II} Single-Ion Magnets. *Eur. J. Chem* **2020**, *26*, 14036−14058.
(40) Tupolova, Y. P.; Shcherbakov, I. N.; Korchagin, D. V.; Tkachev, V. V.; Lebedev, V. E.; Popov, L. D.; Zakharov, K. V.; Vasiliev, A. N.; Palii, A. V.; Aldoshin, S. M. Fine-Tuning of Uniaxial Anisotropy and Slow Relaxation of Magnetization in the Hexacoordinate Co(II) Complexes with Acidoligands. *J. Phys. Chem. C* **2020**, *124*, 25957−25966.
(41) Wang, X.-Y.; Avendaño, C.; Dunbar, K. R. Molecular Magnetic Materials Based on 4*d* and 5*d* Transition Metals. *Chem. Soc. Rev* **2011**, *40*, 3213−3238.
(42) Zabala-Lekuona, A.; Seco, J. M.; Colacio, E. Single-Molecule Magnets: From Mn_{12}-ac to dysprosium metallocenes, a travel in time. *Coord. Chem. Rev* **2021**, *441*, 213984.

Downloaded from pubs.acs.org/inoca/article-pdf/65/41/24492/6737108/acs.inorgchem.6c04158.pdf by FLORIDA STATE UNIV user on 02 November 2026

https://doi.org/10.1021/acs.inorgchem.6c04158
Inorg. Chem. 2026, 65, 24492−24504

(43) Zhuo, Z.; Li, G.-L.; Huang, Y.-G. Understanding Magneto-Structural Correlations Toward Design of Molecular Magnets. *Adv. Struct. Chem.* **2021**, *2*, 777−832.
(44) Bone, A. N.; Widener, C. N.; Moseley, D. H.; Liu, Z.; Lu, Z.; Cheng, Y.; Daemen, L. L.; Ozerov, M.; Telser, J.; Thirunavukkuarasu, K.; et al. Applying Unconventional Spectroscopies to the Single-Molecule Magnets $Co(PPh_3)_2X_2$ (X = Cl, Br, I): Unveiling Magnetic Transitions and Spin-Phonon Coupling. *Eur. J. Chem.* **2021**, *27*, 11110−11125.
(45) Tin, P.; Bone, A. N.; Bui, N. N.; Zhang, Y.-Q.; Chang, T.; Moseley, D. H.; Ozerov, M.; Krzystek, J.; Cheng, Y.; Daemen, L. L.; et al. Advanced Spectroscopic and Computational Studies of a Cobalt(II) Coordination Polymer with Single-Ion-Magnet Properties. *J. Phys. Chem. C* **2022**, *126*, 13268−13283.
(46) Ferrando-Soria, J.; Vallejo, J.; Castellano, M.; Martínez-Lillo, J.; Pardo, E.; Cano, J.; Castro, I.; Lloret, F.; Ruiz-García, R.; Julve, M. Molecular magnetism, quo vadis? A historical perspective from a coordination chemist viewpoint. *Coord. Chem. Rev* **2017**, *339*, 17−103.
(47) Chiozzone, R.; González, R.; Kremer, C.; De Munno, G.; Cano, J.; Lloret, F.; Julve, M.; Faus, J. S. Crystal Structure, and Magnetic Properties of Tetraphenylarsonium Tetrachloro(oxalato)rhenate(IV) and Bis(2,2'-bipyridine)tetrachloro(μ-oxalato)copper(II)rhenium-(IV). *Inorg. Chem* **1999**, *38*, 4745−4752.
(48) Cuevas, A.; Geis, L.; Pintos, V.; Chiozzone, R.; Sanchíz, J.; Hummert, M.; Schumann, H.; Kremer, C. S. Molecular Structure and Magnetic Properties of a Rhenium(IV) Compound with Catechol. *J. Mol. Struct* **2009**, *921*, 80−84.
(49) Tomkiewicz, A.; Bartczak, T. J.; Kruszyński, R.; Mroziński, J. Magnetic Properties, Crystal and Molecular Stucture of $(NBu_4)_2[ReCl_4(ox)]$. *J. Mol. Struct* **2001**, *595*, 225−231.
(50) Martínez-Lillo, J.; Mastropietro, T. F.; Lhotel, E.; Paulsen, C.; Cano, J.; De Munno, G.; Faus, J.; Lloret, F.; Julve, M.; Nellutla, S.; et al. Highly Anisotropic Rhenium(IV) Complexes: New Examples of Mononuclear Single-Molecule Magnets. *J. Am. Chem. Soc.* **2013**, *135*, 13737−13748.
(51) Martínez-Lillo, J.; Faus, J.; Lloret, F.; Julve, M. Towards Multifunctional Magnetic Systems Through Molecular-Programmed Self Assembly of Re(IV) Metalloligands. *Coord. Chem. Rev* **2015**, *289-290*, 215−237.
(52) Pedersen, K. S.; Bendix, J.; Tressaud, A.; Durand, E.; Weihe, H.; Salman, Z.; Morsing, T. J.; Woodruff, D. N.; Lan, Y.; Wernsdorfer, W.; et al. Iridates from the Molecular Side. *Nat. Commun.* **2016**, *7*, 12195.
(53) Sanchis-Perucho, A.; Martínez-Lillo, J. Ferromagnetic Exchange Interaction in a New Ir(IV)−Cu(II) Chain Based on the Hexachloroiridate(iv) Anion. *Dalton Trans* **2019**, *48*, 13925−13930.
(54) Su, Q.-Q.; Fan, K.; Huang, X.-D.; Xiang, J.; Cheng, S.-C.; Ko, C.-C.; Zheng, L.-M.; Kurmoo, M.; Lau, T.-C. Field-Induced Slow Magnetic Relaxation in Low-Spin $S = 1/2$ Mononuclear Osmium(V) Complexes. *Dalton Trans* **2020**, *49*, 4084−4092.
(55) Trop, H. S.; Davison, A.; Carey, G. H.; DePamphilis, B. V.; Jones, A. G.; Davis, M. A. Electrochemical Studies on Halide and Pseudo-Halide Complexes of Technetium and Rhenium. *J. Inorg. Nucl. Chem* **1979**, *41*, 271−272.
(56) Watt, G. W.; Thompson, R. J.; Gibbons, J. M. Potassium Hexachlororhenate(IV) and Potassium Hexabromorhenate(IV). *Inorg. Synth* **1963**, *7*, 189.
(57) Das, A.; Das, U.; Das, A. K. Relativistic effects on the chemical bonding properties of the heavier elements and their compounds. *Coord. Chem. Rev* **2023**, *479*, 215000.
(58) Freedman, D. E.; Jenkins, D. M.; Iavarone, A. T.; Long, J. R. A Redox-Switchable Single-Molecule Magnet Incorporating $[Re(CN)_7]^{3-}$. *J. Am. Chem. Soc* **2008**, *130*, 2884−2885.
(59) Zadrozny, J. M.; Freedman, D. E.; Jenkins, D. M.; Harris, T. D.; Iavarone, A. T.; Mathonière, C.; Clérac, R.; Long, J. R. Slow Magnetic Relaxation and Charge-Transfer in Cyano-Bridged Coordination Clusters Incorporating $[Re(CN)_7]^{3-/4-}$. *Inorg. Chem* **2010**, *49*, 8886−8896.
(60) Schelter, E. J.; Prosvirin, A. V.; Dunbar, K. R. Molecular Cube of Re^{II} and Mn^{II} That Exhibits Single-Molecule Magnetism. *J. Am. Chem. Soc* **2004**, *126*, 15004−15005.
(61) Boča, R. Zero-Field Splitting in Metal Complexes. *Coord. Chem. Rev* **2004**, *248*, 757−815.
(62) Deaton, J. C.; Gebhard, M. S.; Solomon, E. I. Transverse and longitudinal Zeeman effect on [tetraphenylphosphonium tetrachloroferrate(1-)]: assignment of the ligand field transitions and the origin of the $^6A_1$ ground-state zero-field splitting. *Inorg. Chem* **1989**, *28*, 877−889.
(63) Gómez-Coca, S.; Aravena, D.; Morales, R.; Ruiz, E. Large magnetic anisotropy in mononuclear metal complexes. *Coord. Chem. Rev* **2015**, *289-290*, 379−392.
(64) Pyykkö, P. Relativistic Effects in Chemistry: More Common Than You Thought. *Annu. Rev. Phys. Chem* **2012**, *63*, 45−64.
(65) Das, A.; Das, U.; Das, A. K. Relativistic effects on the chemical bonding properties of the heavier elements and their compounds. *Coord. Chem. Rev* **2023**, *479*, 215000.
(66) Sarkar, A.; Tewary, S.; Sinkar, S.; Rajaraman, G. Magnetic Anisotropy in $Co^{II}X_4$ (X = O, S, Se) Single-Ion Magnets: Role of Structural Distortions versus Heavy Atom Effect. *Chem. Asian J* **2019**, *14*, 4696−4704.
(67) Moseley, D. H.; Stavretis, S. E.; Thirunavukkuarasu, K.; Ozerov, M.; Cheng, Y.; Daemen, L. L.; Ludwig, J.; Lu, Z.; Smirnov, D.; Brown, C. M.; et al. Spin−phonon couplings in transition metal complexes with slow magnetic relaxation. *Nat. Commun.* **2018**, *9*, 2572.
(68) Pilbrow, J. R. Effective g values for $S = 3/2$ and $S = 5/2$. *J. Magn. Reson* **1978**, *31*, 479−490.
(69) Gast, P.; Groenen, E. J. J. EPR Interactions − *g*-Anisotropy. *eMagres* **2016**, 1435−1444.
(70) Suturina, E. A.; Maganas, D.; Bill, E.; Atanasov, M.; Neese, F. Magneto-Structural Correlations in a Series of Pseudotetrahedral $[Co^{II}(XR)_4]^{2-}$ Single Molecule Magnets: An *Ab Initio* Ligand Field Study. *Inorg. Chem* **2015**, *54*, 9948−9961.
(71) Rechkemmer, Y.; Breitgoff, F. D.; van der Meer, M.; Atanasov, M.; Hakl, M.; Orlita, M.; Neugebauer, P.; Neese, F.; Sarkar, B.; van Slageren, J. A four-coordinate cobalt(II) single-ion magnet with coercivity and a very high energy barrier. *Nat. Commun* **2016**, *7*, 10467.
(72) Graham, M. J.; Zadrozny, J. M.; Fataftah, M. S.; Freedman, D. E. Forging Solid-State Qubit Design Principles in a Molecular Furnace. *Chem. Mater* **2017**, *29*, 1885−1897.
(73) Pedersen, K. S.; Woodruff, D. N.; Singh, S. K.; Tressaud, A.; Durand, E.; Atanasov, M.; Perlepe, P.; Ollefs, K.; Wilhelm, F.; Mathonière, C.; Neese, F.; et al. $[OsF_6]^{x-}$: Molecular Models for Spin-Orbit Entangled Phenomena. *Chem. Eur. J* **2017**, *23*, 11244−11248.
(74) Stavretis, S. E.; Cheng, Y.; Daemen, L. L.; Brown, C. M.; Moseley, D. H.; Bill, E.; Atanasov, M.; Ramirez-Cuesta, A. J.; Neese, F.; Xue, Z.-L. Probing Magnetic Excitations in Co^{II} Single-Molecule Magnets by Inelastic Neutron Scattering. *Eur. J. Inorg. Chem* **2019**, *2019*, 1119−1127.
(75) Stavretis, S. E.; Moseley, D. H.; Fei, F.; Cui, H.-H.; Cheng, Y.; Podlesnyak, A. A.; Wang, X.; Daemen, L. L.; Hoffmann, C. M.; Ozerov, M.; Lu, Z.; et al. Spectroscopic Studies of the Magnetic Excitation and Spin-Phonon Couplings in a Single-Molecule Magnet. *Chem. Eur. J* **2019**, *25*, 15846−15857.
(76) Thomsen, M. K.; Nyvang, A.; Walsh, J. P. S.; Bunting, P. C.; Long, J. R.; Neese, F.; Atanasov, M.; Genoni, A.; Overgaard, J. Insights into Single-Molecule-Magnet Behavior from the Experimental Electron Density of Linear Two-Coordinate Iron Complexes. *Inorg. Chem* **2019**, *58*, 3211−3218.
(77) Moseley, D. H.; Stavretis, S. E.; Zhu, Z.; Guo, M.; Brown, C. M.; Ozerov, M.; Cheng, Y.; Daemen, L. L.; Richardson, R.; Knight, G.; et al. Inter-Kramers Transitions and Spin−Phonon Couplings in a Lanthanide-Based Single-Molecule Magnet. *Inorg. Chem.* **2020**, *59*, 5218−5230.
(78) Widener, C. N.; Bone, A. N.; Ozerov, M.; Richardson, R.; Lu, Z.; Thirunavukkuarasu, K.; Smirnov, D.; Chen, X.-T.; Xue, Z.-L.

Downloaded from pubs.acs.org/inoca/article-pdf/65/41/24492/6737108/acs.inorgchem.6c04158.pdf by FLORIDA STATE UNIV user on 02 November 2026

https://doi.org/10.1021/acs.inorgchem.6c04158
Inorg. Chem. 2026, 65, 24492−24504

Direct Observation of Magnetic Transitions in a Nickel(II) Complex with Large Anisotropy. *Chin. J. Inorg. Chem* **2020**, *35*, 1149−1156.
(79) Moseley, D. H.; Liu, Z.; Bone, A. N.; Stavretis, S. E.; Singh, S. K.; Atanasov, M.; Lu, Z.; Ozerov, M.; Thirunavukkuarasu, K.; Cheng, Y.; et al. Comprehensive Studies of Magnetic Transitions and Spin−Phonon Couplings in the Tetrahedral Cobalt Complex $Co(AsPh_3)_2I_2$. *Inorg. Chem.* **2022**, *61*, 17123−17136.
(80) Tin, P.; Jenkins, M. J.; Xing, J.; Caci, N.; Gai, Z.; Jin, R.; Wessel, S.; Krzystek, J.; Li, C.; Daemen, L. L.; et al. Haldane topological spin-1 chains in a planar metal-organic framework. *Nat. Commun.* **2023**, *14*, 5454.
(81) Gupta, S. K.; Rao, S. V.; Demeshko, S.; Dechert, S.; Bill, E.; Atanasov, M.; Neese, F.; Meyer, F. Air-stable four-coordinate cobalt(II) single-ion magnets: experimental and *ab initio* ligand field analyses of correlations between dihedral angles and magnetic anisotropy. *Chem. Sci* **2023**, *14*, 6355−6374.
(82) Carbery, W. P.; Verma, A.; Turner, D. B. Spin−Orbit Coupling Drives Femtosecond Nonadiabatic Dynamics in a Transition Metal Compound. *J. Phys. Chem. Lett* **2017**, *8*, 1315−1322.
(83) Sharutin, V. CCDC 850320: Experimental Crystal Structure Determination. *CSD Commun.* **2016**. https://doi.org/10.5517/ccdc.csd.ccxjtpx
(84) Alvarez, S.; Alemany, P.; Casanova, D.; Cirera, J.; Llunell, M.; Avnir, D. Shape maps and polyhedral interconversion paths in transition metal chemistry. *Coord. Chem. Rev* **2005**, *249*, 1693−1708.
(85) Casanova, D.; Cirera, J.; Llunell, M.; Alemany, P.; Avnir, D.; Alvarez, S. Minimal Distortion Pathways in Polyhedral Rearrangements. *J. Am. Chem. Soc* **2004**, *126*, 1755−1763.
(86) Alvarez, S. Distortion Pathways of Transition Metal Coordination Polyhedra Induced by Chelating Topology. *Chem. Rev* **2015**, *115*, 13447−13483.
(87) Hand, A. T.; Watson-Sanders, B. D.; Xue, Z.-L. Spectroscopic techniques to probe magnetic anisotropy and spin−phonon coupling in metal complexes. *Dalton Trans* **2024**, *53*, 4390−4405.
(88) Brackett, G. C.; Richards, P. L.; Caughey, W. S. Far-Infrared Magnetic Resonance in Fe(III) and Mn(III) Porphyrins, Myoglobin, Hemoglobin, Ferrichrome A, and Fe(III) Dithiocarbamates. *J. Chem. Phys* **1971**, *54*, 4383−4401.
(89) Brackett, G. C. *Far-Infrared Magnetic Resonance in Fe(III) and Mn(III) Porphyrins, Myoglobin, Hemoglobin, Ferrichrome A, and Fe(III) Dithiocarbamates. Ph.D. dissertation*, University of California, Berkeley, 1970.
(90) Krzystek, J.; Telser, J. Measuring giant anisotropy in paramagnetic transition metal complexes with relevance to single-ion magnetism. *Dalton Trans* **2016**, *45*, 16751−16763.
(91) Schwoerer, M.; Wolf, H. C. Molecular and Lattice Dynamics in Organic Molecular Crystals. In *Organic Molecular Solids*; Wiley, 2007.
(92) Dove, M. T. *Introduction to Lattice Dynamics*; Cambridge University Press, 1993.
(93) Mitchell, P. C. H.; Parker, S. F.; Ramirez-Cuesta, A. J.; Tomkinson, J. *Vibrational Spectroscopy with Neutrons: with Applications in Chemistry, Biology, Materials Science and Catalysis*; World Scientific Publishing Company, 2005.
(94) Xue, Z.-L.; Ramirez-Cuesta, A. J.; Brown, C. M.; Calder, S.; Cao, H.; Chakoumakos, B. C.; Daemen, L. L.; Huq, A.; Kolesnikov, A. I.; Mamontov, E.; et al. Neutron Instruments for Research in Coordination Chemistry. *Eur. J. Inorg. Chem.* **2019**, *2019*, 1065−1089.
(95) Weil, J. A.; Bolton, J. R. Electron Paramagnetic Resonance. In *Elementary Theory and Practical Applications*; Wiley, 2007.
(96) Chilton, N. F.; Anderson, R. P.; Turner, L. D.; Soncini, A.; Murray, K. S. PHI: A powerful new program for the analysis of anisotropic monomeric and exchange-coupled polynuclear *d*- and *f*-block complexes. *J. Comput. Chem* **2013**, *34*, 1164−1175.
(97) Reta, D.; Chilton, N. F. Uncertainty estimates for magnetic relaxation times and magnetic relaxation parameters. *Phys. Chem. Chem. Phys* **2019**, *21*, 23567−23575.
(98) Aravena, D.; Ruiz, E. Spin dynamics in single-molecule magnets and molecular qubits. *Dalton Trans* **2020**, *49*, 9916−9928.
(99) Feast, G. C.; Haestier, J.; Page, L. W.; Robertson, J.; Thompson, A. L.; Watkin, D. J. An unusual methylene aziridine refined in $P2_1/c$ and the nonstandard setting $P2_1/n$. *Acta Cryst* **2009**, *65*, o635−o638.
(100) Stavretis, S. E.; Atanasov, M.; Podlesnyak, A. A.; Hunter, S. C.; Neese, F.; Xue, Z.-L. Magnetic Transitions in Iron Porphyrin Halides by Inelastic Neutron Scattering and *Ab Initio* Studies of Zero-Field Splittings. *Inorg. Chem* **2015**, *54*, 9790−9801.
(101) Maple software:https://www.maplesoft.com/products/Maple/
(102) Drago, R. S. *Physical Methods in Chemistry*; W. B. Saunders, 1977.
(103) Figgis, B. N.; Hitchman, M. A. *Ligand Field Theory and Its Applications*; Wiley, 2000.
(104) Singh, S. K.; Eng, J.; Atanasov, M.; Neese, F. Covalency and chemical bonding in transition metal complexes: An *ab initio* based ligand field perspective. *Coord. Chem. Rev* **2017**, *344*, 2−25.
(105) Gerloch, M.; Hanton, L. R.; Manning, M. R. Tetrahedral complexes of nickel(II): electronic spectra, σ and π bonding, and the electroneutrality principle. *Inorg. Chim. Acta* **1981**, *48*, 205−214.
(106) Rulfs, C. L.; Meyer, R. J. Rhenium(IV) Compounds: Synthesis and Properties. *J. Am. Chem. Soc* **1955**, *77*, 4505−4507.
(107) Neese, F. The ORCA program system. *WIREs Comput. Mol. Sci* **2012**, *2*, 73−78.
(108) Neese, F. Software update: the ORCA program system, version 4.0. *WIREs Comput. Mol. Sci* **2018**, *8*, No. e1327.
(109) Neese, F.; Wennmohs, F.; Becker, U.; Riplinger, C. The ORCA quantum chemistry program package. *J. Chem. Phys* **2020**, *152*, 224108.
(110) Siegbahn, P.; Heiberg, A.; Roos, B.; Levy, B. A Comparison of the Super-CI and the Newton-Raphson Scheme in the Complete Active Space SCF Method. *Phys. Scr* **1980**, *21*, 323−327.
(111) Siegbahn, P. E. M.; Almlöf, J.; Heiberg, A.; Roos, B. O. The complete active space SCF (CASSCF) method in a Newton−Raphson formulation with application to the HNO molecule. *J. Chem. Phys* **1981**, *74*, 2384−2396.
(112) Roos, B. O.; Taylor, P. R.; Sigbahn, P. E. M. A complete active space SCF method (CASSCF) using a density matrix formulated super-CI approach. *Chem. Phys* **1980**, *48*, 157−173.
(113) Angeli, C.; Cimiraglia, R.; Evangelisti, S.; Leininger, T.; Malrieu, J.-P. Introduction of n-electron valence states for multi-reference perturbation theory. *J. Chem. Phys* **2001**, *114*, 10252−10264.
(114) Angeli, C.; Cimiraglia, R. Multireference perturbation configuration interaction V. Third-order energy contributions in the Møller−Plesset and Epstein−Nesbet partitions. *Theor. Chem. Acc* **2002**, *107*, 313−317.
(115) Angeli, C.; Cimiraglia, R.; Malrieu, J.-P. N-electron valence state perturbation theory: a fast implementation of the strongly contracted variant. *Chem. Phys. Lett* **2001**, *350*, 297−305.
(116) Hess, B. A. Relativistic electronic-structure calculations employing a two-component no-pair formalism with external-field projection operators. *Phys. Rev. A* **1986**, *33*, 3742−3748.
(117) Weigend, F. Accurate Coulomb-fitting basis sets for H to Rn. *Phys. Chem. Chem. Phys* **2006**, *8*, 1057−1065.
(118) Weigend, F.; Ahlrichs, R. Balanced basis sets of split valence, triple zeta valence and quadruple zeta valence quality for H to Rn: Design and assessment of accuracy. *Phys. Chem. Chem. Phys* **2005**, *7*, 3297−3305.
(119) Noro, T.; Sekiya, M.; Koga, T. Segmented contracted basis sets for atoms H through Xe: Sapporo-(DK)-nZP sets (n = D, T, Q). *Theor. Chem. Acc* **2012**, *131*, 1124.
(120) Atanasov, M.; Ganyushin, D.; Sivalingam, K.; Neese, F. A Modern First-Principles View on Ligand Field Theory Through the Eyes of Correlated Multireference Wavefunctions. *Struct. Bond* **2011**, *143*, 149−220.

Downloaded from pubs.acs.org/inocaj/article-pdf/65/41/24492/6737108/acs.inorgchem.6c04158.pdf by FLORIDA STATE UNIV user on 02 November 2026

https://doi.org/10.1021/acs.inorgchem.6c04158
Inorg. Chem. 2026, 65, 24492−24504